

Laura M. Beck

# High-Pressure Direct-Injection Dual Fuel Engine: Evaluation for performance and emission potential by injector modeling and simulation

Master's thesis in Marine Technology

Supervisor: Professor Eilif Pedersen

June 2020



Laura M. Beck

# High-Pressure Direct-Injection Dual Fuel Engine: Evaluation for performance and emission potential by injector modeling and simulation

Master's thesis in Marine Technology  
Supervisor: Professor Eilif Pedersen  
June 2020

Norwegian University of Science and Technology  
Faculty of Engineering  
Department of Marine Technology



Norwegian University of  
Science and Technology



# MASTER THESIS IN MARINE ENGINEERING

FALL 2020

FOR

STUD. TECHN. LAURA M. BECK

## HIGH-PRESSURE DIRECT-INJECTION DUAL FUEL ENGINE - EVALUATION FOR PERFORMANCE AND EMISSION POTENTIAL BY INJECTOR MODELING AND SIMULATION

### *Work description*

Marine engines are subject to increasingly strict regulations governing emissions, and these laws motivate engineers to more effectively use alternative fuels, including natural gas (NG) and hydrogen. Application of NG in low pressure dual fuel (LPDF) engines is already widely in use, but any emissions advantages of this clean and low-carbon fuel are reduced by the increase in harmful hydrocarbon emissions that exist in the form of methane slip. The high-pressure dual fuel (HPDF) engine can drastically reduce or eliminate methane slip by directly injecting NG rather than introducing it to the combustion chamber with the intake air. A significant challenge to HPDF engine development is the specialized injector required to inject high-pressure gaseous fuel into the cylinder. Pressure waves and flow irregularities must be investigated, modeled, and accounted for when designing the injector to guarantee predictable and controllable combustion. This master's thesis will focus on modeling the flow of NG, simplified to its main component of methane, through a preliminary design of an injector supplied by SINTEF. Reviewing this design by modeling and simulation will produce an evaluation of performance as-is as well as recommendations for modification to ensure the desired flow and cylinder penetration.

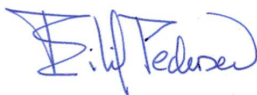
### *Scope of work:*

1. Conduct a design review of the given injector model and investigate how changing parameters impacts the injector's performance.
2. Develop 20-Sim models to simulate injector prototypes.
3. Use simulations of different injector port sizes and opening profiles in a 20-Sim model to improve the injector internal pressure wave simulation.
4. Investigate methane flow through the injector into the cylinder for a range of slight adjustments to internal injector dimensions.
5. Evaluate proposed safety devices for the injector.

The report shall be written in English and edited as a research report including literature survey, description of mathematical models, description of control algorithms, simulations results, discussion and conclusion including a proposal for further work.

The Department of Marine Technology, NTNU, can use the results freely in its research work by referring to the students work.

Trondheim January, 2020



Eilif Pedersen  
Associate Professor (Advisor)



---

## Preface

This thesis is submitted as the final requirement for completion of a two-year Master's Program in Marine Technology with a specialization in Marine Engineering at the Norwegian University of Science and Technology in Trondheim, Norway. This topic was selected as a result of the author's interest in improving the environmental impact of ships using methods available for widespread use in the near future.

The study and research conducted for this project occurred from January to June of 2020 under the supervision of Professor Eilif Pedersen.

The intended audience for this document is a reader with basic knowledge of engine operation and computer modeling of fluid systems.



---

## Acknowledgement

I sincerely thank my supervisor, Eilif Pedersen, for his academic and research guidance over my two-year study experience at NTNU. Even in the midst of a global pandemic that did not allow us to work on campus, he ensured my understanding of the topics in this thesis and I am very grateful for his investment in my education.

I am also grateful to the US-Norway Fulbright Foundation for providing me with the opportunity to pursue and complete this degree in Norway. The additional opportunities for growth presented by living abroad enhanced my study experience and allowed me to develop simultaneously as an engineer and a global citizen.

Finally, I am grateful to the US Coast Guard for allowing me the time away from my regular duties to advance my education. I am proud to be a member of a service that places such a high value in its people.



---

## Abstract

Natural gas is a promising alternative fuel for marine engines that must comply with strict international emissions regulations. The current standard for these engines is the low-pressure dual fuel arrangement usually associated with high levels of harmful hydrocarbon emissions. Alternatively, the high-pressure dual fuel arrangement has the potential to eliminate these emissions which makes it one of the best options to comply with the International Maritime Organization's emissions guidelines for ships. Direct injection of gaseous fuel into the cylinder requires a novel fuel injector. A prototype in development by L'Orange was modeled for this thesis using bond graph theory and the modeling and simulation program 20-Sim. The internal dimensions of this complex injector were modified to understand how further iterations of the design process may influence how the injector functions, specifically concerning mass flow into the cylinder during injection and pressure fluctuations within the injector. The largest volumes were confirmed to have the most significant influence on injector performance, indicating that if these components require significant re-sizing, more advanced simulations may be required to ensure adequate flow for different engine requirements. A safety shut-off device proposed by the manufacturer was also evaluated for effectiveness. Simulations indicate that this quick-closing device activated by a significant decrease in downstream pressure is not an effective safety system to prevent excessive fuel buildup in the cylinder during a failure of a needle stuck in the open position.



---

# Contents

<b>Preface</b> . . . . .	<b>iii</b>
<b>Acknowledgement</b> . . . . .	<b>v</b>
<b>Abstract</b> . . . . .	<b>vii</b>
<b>Contents</b> . . . . .	<b>ix</b>
<b>Nomenclature</b> . . . . .	<b>xiii</b>
<b>List of Figures</b> . . . . .	<b>xvii</b>
<b>List of Tables</b> . . . . .	<b>xxi</b>
<b>1 Introduction</b> . . . . .	<b>1</b>
<b>2 Background</b> . . . . .	<b>3</b>
2.1 Regulations Driving Innovation . . . . .	3
2.1.1 Carbon Dioxide and Nitrogen Oxides . . . . .	4
2.2 Outlook . . . . .	6
<b>3 Dual Fuel Engine Development</b> . . . . .	<b>9</b>
<b>4 Fuel Injectors</b> . . . . .	<b>15</b>
4.1 Fuel Injectors for Marine Engines . . . . .	15
4.2 An Existing HP Gas Injector Bond Graph Model . . . . .	17
<b>5 Bond Graph Theory</b> . . . . .	<b>19</b>
5.1 Theoretical Basis . . . . .	19
5.2 Bond Graph Elements . . . . .	20
5.2.1 1-Port Elements . . . . .	20
5.2.2 Multi-port Junction Elements and Causality . . . . .	22
5.2.3 Multi-port Fields . . . . .	23
5.3 Pseudo-Bond Graphs for Thermodynamic Modeling . . . . .	23
5.4 Injector Interior: Control Volume Modeling . . . . .	24
<b>6 Methods</b> . . . . .	<b>29</b>
<b>7 Building the Simplified Model</b> . . . . .	<b>31</b>
7.1 Boundary Conditions . . . . .	32
7.2 Valves . . . . .	33
7.3 Cylindrical Volumes . . . . .	34
7.4 Simple 20-Sim Model . . . . .	34

---

<b>8</b>	<b>Initial Parameters and Assumptions</b>	<b>37</b>
8.1	System Initial Conditions	37
8.2	Injection Profile	38
8.3	Heat Transfer	39
8.4	Loss Coefficients	43
8.4.1	Isentropic Conditions	43
8.4.2	Adiabatic Conditions	45
8.4.3	Concluding Remarks	47
<b>9</b>	<b>Testing the Simplified Model</b>	<b>49</b>
9.1	Parameter Sweep Simulations	49
9.2	Pressure Waves	54
9.2.1	Pressure Drop During Injection	57
<b>10</b>	<b>Application to Advanced Model</b>	<b>59</b>
10.1	Internal Volumes	60
10.1.1	Variation in Top Volume	61
10.1.2	Volume 1 Changes	63
10.1.3	Volume 2 Changes	64
10.1.4	Volume 3 Changes	64
10.1.5	Sac Volume Changes	65
10.1.6	Top Valve Use	67
10.2	Inlet Pressure	68
10.3	Injection Duration	70
10.4	Failure Analysis	73
10.4.1	Closed Needle Comparison	73
10.4.2	Mass Flow Considerations	76
10.4.3	Pressure Drop and Quick Closing Valve	79
10.4.4	Gas Velocity	83
<b>11</b>	<b>Summary</b>	<b>87</b>
11.1	Conclusions	87
11.1.1	Simple Model	87
11.1.2	Advanced Model	88
11.2	Discussion and Further Work	89
	<b>Bibliography</b>	<b>91</b>
	<b>A Model Input Parameters</b>	<b>95</b>
	<b>Appendices</b>	<b>94</b>

---

---

**B 20-Sim Pipe Code . . . . . 97**

---



---

## Nomenclature

T	Temperature
P	Pressure
m	Mass
$\dot{m}$	Mass Flow
L	Length
D/diam	Diameter
A	Area
$\rho$	density
u/U	Velocity
E	Total Internal Energy
e	Specific Internal Energy
$\dot{E}$	Energy Flow
H	Total Enthalpy
h	Specific Enthalpy

---

$\mu$	Kinematic Viscosity
$\dot{Q}$	Total Rate of Heat Addition
$\dot{q}$	Specific Rate of Heat Addition
Re	Reynolds Number
Pr	Prandtl Number
Nu	Nusselt Number
$\kappa$	Specific Heat Ratio
$C_p$	Specific Heat at Constant Pressure
$\alpha$	Thermal Diffusivity
$\lambda$	Thermal Conductivity
$\tau$	Frictional Shear Stress Tensor
Hz	Hertz
p(t)	momentum
q(t)	displacement
e(t)	effort
f(t)	flow

---

IMO	International Maritime Organization
MEPC	Marine Environmental Protection Committee
MARPOL	The International Convention for the Prevention of Pollution from Ships
ECA	Emissions Control Area
EEDI	Energy Efficiency Design Index
LBSI	Lean Burn Spark Ignition
LNG/NG	Liquified Natural Gas
MDO	Marine Diesel Oil
DF	Dual Fuel
GD	Gas Diesel Engine
HPDF	High Pressure Dual Fuel
LPDF	Low Pressure Dual Fuel



---

## List of Figures

1	Emission Reduction Potential of LNG as fuel compared to MDO (Vilmar Aeligsoy & Valberg. (2011)) . . . . .	6
2	4-Stroke Dual-Fuel Engine Fuel Injection Schematic (Ohashi (2015))	10
3	Comparison of Natural Gas-fueled Engine Cycles (Vilmar Aeligsoy & Valberg. (2011)) . . . . .	11
4	High Pressure Dual Fuel Injector with 3 Gas Needles (Marintek (2019)) . . . . .	12
5	Gas Injector Bond Graph Model (Krivopolianskii (2019)) . . . . .	17
6	Tetrahedron of State . . . . .	20
7	Tetrahedron of State with 1-Port Elements . . . . .	21
8	Zero-Junction . . . . .	22
9	One-Junction . . . . .	22
10	Pseudo-Bond Graph Variables . . . . .	24
11	Control Volume Indexing Convention . . . . .	26
12	Simplified Sketch of Internals of the L'Orange Prototype High Pressure Gas Fuel Injector . . . . .	31
13	Variable Pressure Profile for Se Element . . . . .	33
14	Simple Injector Model . . . . .	34
15	Motion Profile for Injector Needle Opening . . . . .	38
16	Simple Pipe Model for Heat Transfer Investigation . . . . .	39
17	Heat transfer coefficient for a range of gas velocities . . . . .	42
18	Comparison of Temperatures with and without Heat Transfer in Pipe	42
19	Comparison of Temperatures different tfact Parameter Values . . . . .	44
20	Temperature Effects of Changing Adiabatic Scaling Parameter . . . . .	46
21	Pressure Effects of Changing Adiabatic Scaling Parameter . . . . .	46
22	Velocity Effects of Changing Adiabatic Scaling Parameter . . . . .	47
23	Parameter Sweep Results for Upper Volume (V4) . . . . .	50
24	Approximate Representation of Volume Injected per Cycle . . . . .	51
25	Parameter Sweep Results for Pipe Volume (V23) . . . . .	52
26	Parameter Sweep Results for Ring Volume (V1) . . . . .	53

---

27	Upper Volume (V4) . . . . .	53
28	Pipe Volume (V23) . . . . .	54
29	Ring Volume (V1) . . . . .	54
30	Ring Volume Pressure for Decreasing Pipe Diameter . . . . .	55
31	Ring Volume Pressure for Increasing Pipe Diameter . . . . .	56
32	Pressure Variation Within Pipe . . . . .	57
33	Pressure Drop During Injection for Changing Pipe Volume . . . . .	58
34	Pressure Drop During Injection for Changing Ring and Upper Volumes . . . . .	58
35	Simplified Graphic of Advanced Model . . . . .	59
36	Advanced Model in 20-Sim . . . . .	60
37	Fuel Injected Per Cycle Represented as a Percentage of Injector Volume . . . . .	61
38	Mass Flow into Cylinder for Changing Volume 0_1 . . . . .	62
39	Mass Flow into Cylinder for Changing Volume 0_2 . . . . .	63
40	Mass Flow into Cylinder for Changing Volumes 1_1 and 1_2 . . . . .	63
41	Mass Flow into Cylinder for Changing Volumes 2_1, 2_2, and 2_3 . . . . .	64
42	Mass Flow into Cylinder for Changing Volumes 3_1, 3_2, and 3_3 . . . . .	65
43	Mass Flow into Cylinder for Changing Sac Volumes . . . . .	65
44	Mass per Injection for Changing Sac Volumes . . . . .	66
45	Pressure Drop Before Needle for Changing Sac Volumes . . . . .	66
46	Slight Increase of Mass into Cylinder for Increasing Upper Pipe Size . . . . .	67
47	Similar Gas Velocity for Changing Upper Pipe Size . . . . .	68
48	Slight Decrease in Pre-Needle Pressure Fluctuations for Changing Upper Pipe Size . . . . .	68
49	Mass Flow for Changing Initial Pressure . . . . .	69
50	Mass Injected Per Cycle for Changing Initial Pressure . . . . .	69
51	Pressure Drop During Injection for Changing Initial Pressure . . . . .	70
52	Mass Flow for Changing Injection Duration . . . . .	71
53	Mass Injected Per Cycle for Changing Injection Duration . . . . .	71
54	Pressure Drop During Injection for Changing Injection Duration . . . . .	72
55	20-Sim Model Components of Six Pipes Feeding Injector Needles . . . . .	73
56	Comparison of Mass Flow into Cylinder for Inner vs. Outer Needle Stuck Closed . . . . .	75

---

57	Comparison of Mass Flow Out of Individual Needles for Outer vs. Inner Needle Stuck Closed . . . . .	75
58	Mass Flow into Cylinder Comparison for Closed Needle Failure . . . . .	76
59	Mass Accumulated in Cylinder for Closed Needle Failure . . . . .	77
60	Mass Flow Comparison for Open Needle Failure . . . . .	78
61	Mass Accumulated in Cylinder for Open Needle Failure . . . . .	78
62	Proposed Quick Closing Valve Actuation . . . . .	79
63	First Injection . . . . .	80
64	Second Injection . . . . .	80
65	First Injection . . . . .	80
66	Second Injection . . . . .	80
67	Pressure in Volume 0_1 With Failure: Steady State . . . . .	82
68	Pressure in Volume 0_2 With Failure: Steady State . . . . .	82
69	Gas Pipe Velocity: Fully Operational Condition . . . . .	84
70	Gas Pipe Velocity: 1 Injector Needle Stuck Closed . . . . .	85
71	Gas Pipe Velocity: 2 Injector Needles Stuck Closed . . . . .	85
72	Gas Pipe Velocity: 1 Injector Needle Stuck Open . . . . .	86
73	Gas Pipe Velocity: 2 Injector Needles Stuck Open . . . . .	86



---

## List of Tables

1	Input Values for $\alpha(U)$ Calculation . . . . .	41
2	Internal Volume and Diameter Changes for Initial Model Simulations	50
3	Internal Sizes for Advanced Injector Model . . . . .	60
4	Top Pipe Size Assumptions for Optional Top Valve Use . . . . .	67



---

# 1 Introduction

The interconnected global economy depends on the shipping industry to transport 80% of all cargo by volume and over 90% by value between markets around the world. Increased awareness of the negative environmental impacts associated with combustion engines and the desire to reduce anthropogenic climate change has led to the development of new regulations concerning emissions from ships. These regulations drive technological developments in engine design, alternative fuels, and exhaust treatment in an effort to strike a balance between the advantages of global trade and the environmental costs of long-distance transport.

This thesis focuses on one strategy for making the promise of a cleaner petroleum fuel source, natural gas (NG), a reality for the maritime industry: high pressure direct injection for dual-fuel engines. Marine engines fueled by NG do not produce many of the harmful emissions linked to heavy fuel oil including sulfur oxides and particulate matter. Traditionally, when NG is used in marine engines it is as a low-pressure gaseous fuel source mixed with air during the engine's intake stroke. This method often results in significant levels of methane in the exhaust, commonly known as methane slip. Methane emissions are over twenty times as harmful as carbon dioxide emissions, so their presence in exhaust negates many of the emissions advantages of NG over heavy fuel oil. An alternative strategy for NG use is high pressure direct injection (HPDI) of NG which has the potential to eliminate methane slip and enhance combustion efficiency. As international environmental regulations for ships become more demanding, it is of interest to

the entire maritime industry to invest in technologies that reduce the harmful environmental impact of shipping. NG is one of the most viable alternative fuels because it is already available worldwide and has the potential to improve ship emissions on a much shorter timeframe than any other technology currently in development.

The closer focus of this work will be on the specialized fuel injectors required to inject NG at high pressure, approximately 350 bar. A bond graph model built in the modeling and simulation program 20-Sim approximates the preliminary L'Orange fuel injector design and facilitates pre-production design verification. Some of the results of interest are internal pressure oscillations, mass flow rates through each component, and relationships between different design parameters and the performance of the injector. Since this injector is still in development, the size and arrangement of internal volumes may still change before it becomes operational. As such, it is of interest to know how slight and significant changes in the sizes initially chosen impact the injector's performance. ([Beck \(2019\)](#))

---

## 2 Background

### 2.1 Regulations Driving Innovation

The International Maritime Organization (IMO) operates under the authority of the United Nations and creates the regulations that govern the standards of ships around the world. The Marine Environmental Protection Committee (MEPC) within the IMO focuses on regulations pertaining to the environmental impact of ships, specifically concerning pollution into the air and water. The International Convention for the Prevention of Pollution from Ships (MARPOL) is the primary convention governing emissions, with 158 nations representing 99.01% of the world's merchant shipping fleet agreeing to comply with these rules (IMO (2019)). As such, these nations have also agreed to abide by the updates to MARPOL, including enhanced fuel sulfur limitations and engine certification standards for reduced nitrogen oxide and carbon dioxide emissions.

On January 1, 2020, the allowable sulphur content of fuel used onboard ships was limited to just 0.1% by weight in Emission Control Areas (ECA's) close to land and 0.5% elsewhere (IMO (2012b)). Prior to this date, the global limit was the same for ECA's but 3.5% elsewhere. Imposing such a drastic decrease in permissible fuel sulphur content met resistance from the maritime industry and debate as to the best methods to adapt existing ships and fuels to meet the standard. Regulations permit for higher sulphur content fuel to be used if other methods such as after-treatment systems are used to create a lower equivalent method,

however limiting sulphur from the start by using low-sulphur fuel is a far preferred strategy. Secondary methods such as exhaust gas after-treatment systems, or scrubbers, take up valuable space onboard a ship which must be accounted for when considering their application and efficiency.

### 2.1.1 Carbon Dioxide and Nitrogen Oxides

The MEPC introduced the Energy Efficiency Design Index (EEDI) in 2011 to promote efficient machinery that produces less pollution for all applications in commercial ships. In contrast to sulfur regulations that can apply to existing ships, the EEDI applies to ships during their design phase, urging manufacturers and researchers to develop cleaner technologies from the start (IMO (2020)). EEDI regulations are set to achieve a 30% reduction in  $CO_2$  emissions per ton-nautical mile by the year 2025. The focus on reducing  $CO_2$  emissions requires creative thinking from engineers and naval architects to achieve this ambition. From improving hull design to decrease the power requirement for a vessel to changing the fuel to a lower-carbon source, many options exist and are being studied to achieve this goal.

Using fuels with less carbon has a direct relationship to reduced carbon emissions for rather straightforward reasons. The energy extracted from fuel comes from carbon-hydrogen bonds in the fuel molecules. Therefore, natural gas' primary component, methane ( $CH_4$ ), offers the most energy per carbon atom of any other carbon-based fuel since there are very few multi-carbon atom components in this fuel. The chief downside of methane as fuel is the risk of methane slip, un-combusted fuel exiting the engine as emissions which are much more harmful than  $CO_2$  emissions.

In addition to EEDI requirements meant to limit  $CO_2$  emissions, the IMO also regulates  $NO_x$  emissions during the construction phase by certifying different marine diesel engines as Tier I, Tier II, or Tier III. As the tier increases, the emission limit for  $NO_x$  decreases. The tier requirement for a ship is determined by the ship's construction date, with all vessels built after January 1, 2016 being required to meet the strictest requirements, Tier III, while operating inside ECA's. When outside of ECA's, the Tier II limits apply (IMO (2012a)).

While the lower carbon content of methane fuel has a direct relationship to lower  $CO_2$  emissions, using methane as fuel offers an even more significant decrease in  $NO_x$  emissions.  $NO_x$  emission reduction is attributed primarily to the lean, homogeneous combustion that occurs in lean burn spark ignition (LBSI) engines (Vilmar Aeligsoy & Valberg. (2011)). Dual fuel and high pressure gas engines still offer some reduction in  $NO_x$  but not as much as LBSI. On the other hand, LBSI engines are also more susceptible to hydrocarbon emissions (methane slip) than high pressure gas engines. The image below illustrates the emission reduction potential when natural gas (LNG) is used instead of marine diesel oil (MDO). The most significant differences are attributed to the fact that natural gas contains far fewer, nearly negligible, impurities that contribute to  $SO_x$  and particulate emissions.

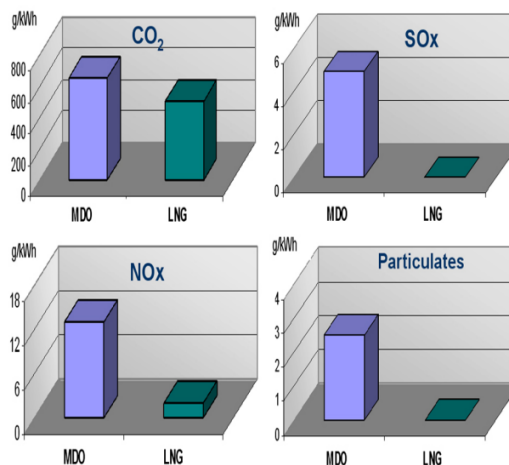


Figure 1: Emission Reduction Potential of LNG as fuel compared to MDO (Vilmar Aeligsoy & Valberg. (2011))

## 2.2 Outlook

Natural gas is gaining popularity as an alternative to diesel fuel in a political environment that encourages the implementation of cleaner fuels because it offers low particulate emissions and better control of  $NO_x$  emissions. The high octane number without additives also makes it a good fuel for use in engines with high compression ratios, but this also means that traditionally, liquid diesel fuel must be used as a pilot fuel. Furthermore, its global availability is increasing, making it both accessible and less expensive than other alternatives, which is significant when fuel makes up a large fraction of a vessel's total operating costs. Due to challenges around retrofitting existing vessels, demand for LNG and thus pricing depends on new-build vessels (Fevre (2018)). As of May 2018, half of the the 254 existing LNG-fueled vessels were in operation with the other half still under construction. These vessels' expected annual fuel consumption is between 1.2

and 3 million tonnes when LNG tanker consumption is excluded (Fevre (2018)). These values have been shown by some studies to increase to up to 30 million tons per year by 2030, a value that reflects an assumption of 10 to 400 new builds each year until 2030 (Fevre (2018)). The high end of this estimate is uncertain since LNG is not the ultimate solution to eliminate carbon emissions, but rather a short-term solution to reduce the environmental impact of ships while completely clean solutions are perfected. It is reasonable to assume some ship owners will delay investment in LNG-fueled vessels in order to invest in cleaner technologies later. But for those urgently needed new-build vessels, LNG offers many advantages over traditional fuels and is a suitable transition technology for the next several decades. (Beck (2019))



---

### 3 Dual Fuel Engine Development

The development of internal combustion engines that use methane as fuel began from a desire to use the natural gas produced as a byproduct of oil extraction from underground. Similarly, it was desirable to use the vapors that naturally boil off from liquefied natural gas (LNG) cargo on LNG tank ships for energy production onboard. These two sources of demand pushed the development of engines that could use LNG, and the dual-fuel engine was the main outcome. Mixing natural gas (NG) with intake air in a traditional diesel engine allowed for reduced diesel fuel oil consumption. Four-stroke dual-fuel engines emerged as the first mature technology; they also had the ability to run on diesel fuel alone to satisfy regulatory requirements for backup fuel arrangements. More recently, in 2010, two-stroke dual-fuel engines emerged for main propulsion on ships. As the technology has developed, the focus shifted from using residual NG to relying on NG as much as possible because of the improved emissions characteristics when this cleaner fuel is used instead of heavy diesel fuel. The image below shows a typical fuel supply setup for a 4-stroke dual-fuel engine. The main and micro-pilot fuel injectors are for diesel fuel while the NG is introduced to the cylinder with the intake air through the gas valve.

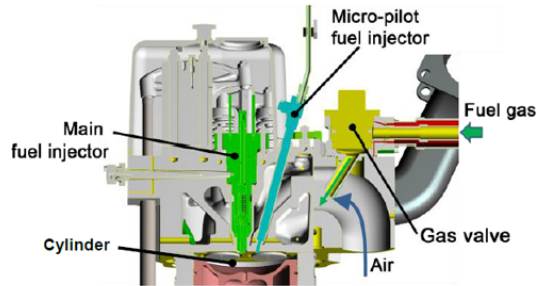


Figure 2: 4-Stroke Dual-Fuel Engine Fuel Injection Schematic (Ohashi (2015))

The main disadvantage of this method stems from the fact that introducing NG into the cylinder with the intake air allows it to be compressed into the many crevices that exist in a cylinder as the piston moves up during the compression stroke. Because the combustion flame cannot propagate in most of these small spaces, the fuel trapped there during compression is exhausted without being burned, contributing to methane emissions that are 28 times more harmful to the environment than carbon dioxide (GHGP (2018)). DF and LBSI engines that operate on the Otto cycle are prone to methane slip.

The dual-fuel arrangement can be retrofitted for existing ships, however the low-load performance is often characterized by high hydrocarbon emissions, bringing into question how much an improvement is really seen from this engine type. The main adjustment that can improve the emissions from engines that use NG is to directly inject the NG rather than mixing the NG with intake air. Additionally, higher injection pressures are associated with reduced soot emissions at middle and high loading (Jingzhou Yu (2013)). While LBSI and DF engines operate on the Otto cycle, high-pressure gas injection engines (GD) operate on the diesel cycle. The image below shows a comparison of these three cycle options.

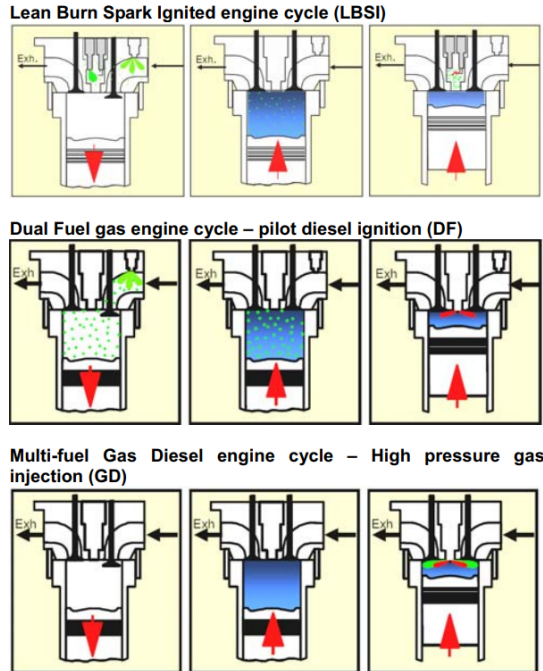


Figure 3: Comparison of Natural Gas-fueled Engine Cycles (Vilmar Aeligsoy & Valberg. (2011))

The LBSI and DF cycles both compress a homogeneous mixture of air and natural gas in the Otto cycle. The GD cycle operates on the diesel cycle, so high pressure NG and diesel pilot fuel are injected after the intake air is compressed alone.

Injecting the gas at the top of the stroke and employing the diesel cycle nearly eliminates methane slip, but this setup requires significant redesign of fuel injector components. Additionally, pilot fuel is still required to ignite the gas, so a combined injector for both the gas and diesel pilot is desired. One preliminary design for this injector is shown in the image below.

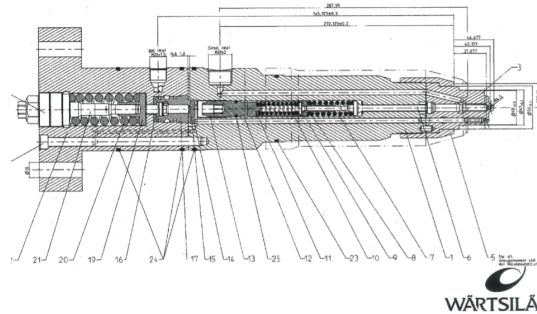


Figure 4: High Pressure Dual Fuel Injector with 3 Gas Needles (Marintek (2019))

The combined fuel injector produces an injection pattern where the gas penetrates further into the cylinder and the diesel pilot fuel is concentrated in the richer area near the injector. This encourages the formation of a diffusion flame as is characteristic in the diesel cycle for compression-ignition engines. The 3-needle configuration as depicted above admits fuel into the cylinder through three passages that each have three openings into the cylinder for nine total gas jets. This design developed by MARINTEK allows adequate flow while maintaining symmetry and ensuring adequate penetration (Marintek (2019)). Increasing the number of jets of NG fuel also aids in fuel/air mixing and thus improves combustion efficiency.

There are several volumes and restrictions inside the injector that the gas flows through before injection into the cylinder. The bond graph model studied later in this thesis allows for the investigation of the effect of changing the internal volumes and the valve opening pattern among other parameters. The purpose for modeling the volumes and restrictions within the injector is to better understand the unique dynamics associated with high pressure gas injection for the proposed injector. As gas flows out of the injector, the internal pressure

---

rapidly drops before the supply of gas acts to re-fill the injector. As such, the volume in the injector must contain a sufficient amount of gas to account for any oscillations and not restrict flow so much that insufficient fuel is admitted to the cylinder. Pressure is the driving force for injection, so the sizing of the injector must be adequate for a plausible range of injection durations for various engine speeds and power levels. In a compression-ignition engine, combustion is controlled by precise control of the amount and timing of fuel injection. Excessive oscillations have the potential to reduce the controllability of combustion which can lead to both inefficient and potentially dangerous situations for combustion. (Beck (2019))

Prior to conducting any simulations, it was hypothesized that the dimensions of the channels inside the injector, modeled as pipes, would have a driving influence on the frequency of pressure fluctuations within the injector. The internal components modeled as volumes where gas accumulates were hypothesized to have less of an effect on pressure fluctuations and more of an effect on changing mass flows into the cylinder. A goal value of approximately 2 grams of gas injected per cycle was used as a metric for evaluating how changing each internal dimension changed the performance of the fuel injector.



---

## 4 Fuel Injectors

In conventional diesel engines, fuel injectors introduce liquid fuel to the cylinder when the piston is close to top dead center as conditions are ideal for auto-ignition. Low pressure dual fuel engines inject natural gas, the primary fuel, in the intake manifold so that it is compressed along with air in the cylinder. For ignition, just a small amount of liquid diesel pilot fuel is injected at the top of the stroke to initiate ignition of the natural gas, or in LBSI engines, a spark is used to ignite the fuel. Compressing the natural gas with air is a process that directly leads to methane slip. Injecting gas at a high pressure at the top of the engine stroke with the pilot fuel thus will decrease the possibility of methane slip.

### 4.1 Fuel Injectors for Marine Engines

Marine engines typically have either common rail injectors or unit injectors. The main difference between the two is that a common rail injector can be controlled independently of the engine, allowing for injection rate and duration to be optimized for the given load profile. Unit injectors are actuated by a cam, and are thus mechanically linked to engine speed and the shape of the cam and cannot be more finely tuned once installed. Dual fuel engines usually use common rail injectors to ensure adequate control of pilot fuel spray which has a direct relationship to emissions properties. Additionally, HPDF engines use a common rail to inject the high pressure gas fuel ([Krivopolianski \(2019\)](#)).

Both LPDF and HPDF engines require pilot fuel injector optimization to ensure

full atomization of the diesel fuel and thus predictable and steady combustion characteristics. As with a typical diesel engine, advancing injection timing and decreasing the amount of pilot fuel injected is associated with a reduction in  $NO_x$  emissions. The cost of this advantage is a slight increase in PM emissions and decreased engine efficiency (Krivopolianskii (2019)).

As with the diesel pilot fuel, the gas injection timing and pressure can be optimized for the desired emissions and power properties. Increased injection pressure allows the gas jet to penetrate further into the cylinder, and thus a greater surface area is exposed for the diffusion flame to create  $NO_x$  gas. A similar effect has been shown when gas injection occurs too far in advance of pilot fuel injection. On the other hand, reduced injection pressure and less penetration extends combustion time and reduces efficiency. (Krivopolianskii (2019))

## 4.2 An Existing HP Gas Injector Bond Graph Model

The theoretical model developed by Vladimir Krivopolianskii for a high pressure gas injector was the starting point for this project's modeling and analysis. His model is shown in the image below and was also created in 20-Sim.

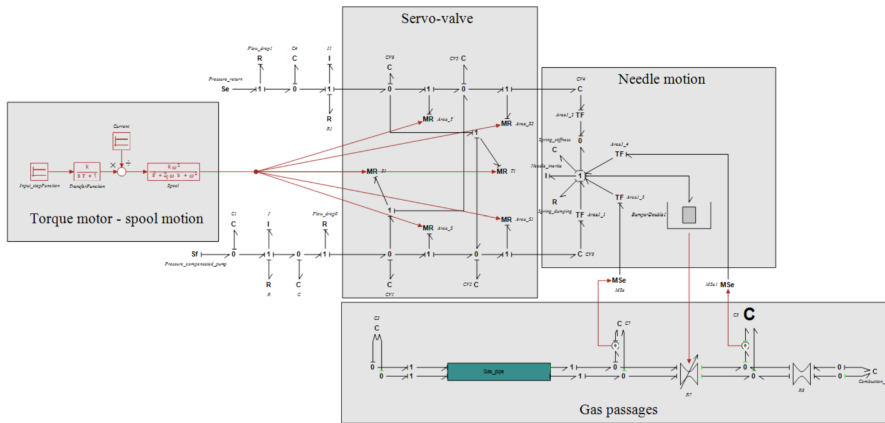


Figure 5: Gas Injector Bond Graph Model (Krivopolianskii (2019))

This model is not based on the L'Orange fuel injector that is the focus of the design review portion of this thesis, but it is useful to understand the different volumes and restrictions that exist in a simplified high pressure gas fuel injector. The gas pipe (green) is the largest volume where gas can accumulate in the injector. The "C" capacitor elements to the right of this pipe represent the volume of gas contained within the valves that lead to the combustion chamber. The valve elements here represent restrictions in the flow toward the cylinder. The elements modeled above the gas pipe and valves in the model simulate the motion of the needle and the control mechanisms for the injector. Krivopolianskii's model was useful to improve the understanding of gas dynamics and modeling and

provided a comprehensive introduction to the strengths of the 20-Sim program. Later models sought to better approximate the actual sizes and geometry in the proposed high pressure gas injector. ([Beck \(2019\)](#))

---

## 5 Bond Graph Theory

The bond graph modeling technique offers many useful advantages for this project. The fuel injector can be divided into several components, including volumes where the gas moves through or is stored, and restrictions that change the flow behavior. Some basic elements used in bond graph modeling are described here. Information beyond the introduction to these elements described in this section can be found in Dean C. Karnopp's textbook ([Karnopp et al. \(2012\)](#)).

### 5.1 Theoretical Basis

A bond graph connects different elements of a model through power bonds which represent effort and flow variables that are transferred without losses between energy ports on those elements. Depending on the system, these variables represent different physical quantities, but no matter the situation, multiplying effort by flow gives power, hence the name "power bond."

$$P(t) = e(t)f(t) \tag{5.1}$$

For the thermodynamic system that is the focus of this thesis, the relevant effort and flow pair is *pressure* and *mass flow*.

Energy variables are also important to describe this dynamic system, these variables are momentum  $[p(t)]$  and displacement  $[q(t)]$ . They are found by inte-

grating the flow and effort variables, respectively.

$$p(t) = \int^t e(t)dt \quad (5.2)$$

$$q(t) = \int^t f(t)dt \quad (5.3)$$

The relations between the energy and power variables are summarized by the tetrahedron of state, developed by Karnopp ([Karnopp et al. \(2012\)](#)).

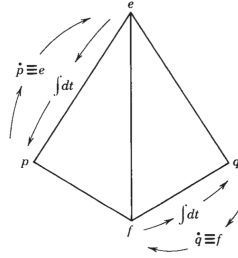


Figure 6: Tetrahedron of State

## 5.2 Bond Graph Elements

Bond graphs can model a wide variety of system types, but the elements that make up the model of any system are consistent. The elements used for modeling in this thesis are divided into two categories: 1-port elements and multi-port elements.

### 5.2.1 1-Port Elements

The 1-port elements in bond graphs represent how different parts of a physical system effect the effort and flow variables moving through the system. These model components include the capacitor (**C**), resistor (**R**), and inertia (**I**) ele-

ments. They are related to effort and flow as well as momentum and displacement by the refined tetrahedron of state shown in the image below.

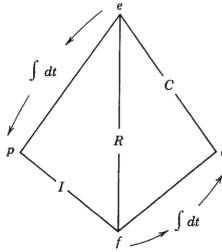


Figure 7: Tetrahedron of State with 1-Port Elements

The capacitor element (**C**) represents the physical relationship between effort and displacement, storing energy in a system as in a storage tank, spring, or electrical capacitor. Capacitor elements are used throughout the fuel injector model to represent volumes of fuel accumulated in different spaces, such as valves and connections. The inertia element (**I**) represents the physical relationship between momentum and flow, such as an object's mass or an inductor. The resistor element (**R**) represents the relationship between effort and flow, dissipating energy as with friction or an electrical resistor. Resistor elements are used throughout the model to represent flow restrictions and friction.

Boundary conditions are established in the model using another kind of 1-port element, the effort source (**Se**). The source element represents an ideal source of some variable, modeling the pressure and temperature inside the cylinder during injection for this project.

### 5.2.2 Multi-port Junction Elements and Causality

Power is transmitted through the model without loss through zero- and one- junctions which conserve flow and effort, respectively. The effort and flow relations for a zero-junction is:

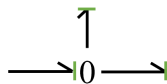


Figure 8: Zero-Junction

$$e_1(t) = e_2(t) = e_3(t) \quad (5.4)$$

$$f_1(t) + f_2(t) + f_3(t) = 0 \quad (5.5)$$

The effort and flow relations for a one-junction is:

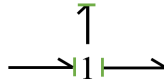


Figure 9: One-Junction

$$f_1(t) = f_2(t) = f_3(t) \quad (5.6)$$

$$e_1(t) + e_2(t) + e_3(t) = 0 \quad (5.7)$$

The green lines drawn perpendicular to one end of each of the power bonds in the images above indicate causality, or from which direction effort is being set on the junction. Similar marks appear on every bond, and certain elements have a preferred causality for the purpose of writing state equations for the dynamic

system. More on this subject can be found in Chapter 3 of [Karnopp et al. \(2012\)](#).

### 5.2.3 Multi-port Fields

C-fields represent the compliance of an element in a system, whether that is a beam bending or a gas accumulator filling. The energy stored in a C-field is:

$$\mathbf{E} = \int_{t_0}^t \sum_{i=1}^n (e_i f_i) dt = \int_{t_0}^t \sum_{i=1}^n (e_i q_i) dt = \int_{q_0}^q \sum_{i=1}^n (e_i \mathbf{q}) dq_i = \int_{q_0}^q \mathbf{e}(\mathbf{q}) d\mathbf{q} = \mathbf{E}(\mathbf{q}) \quad (5.8)$$

IC-fields mix the energy storage properties of the I and C fields. The fuel injector model built for this project involves at least two different energy domains, so the IC field is the most appropriate way to model how the fuel moves through certain volumes within the injector.

While the C-field relates effort to displacement, an I-field relates flow to momentum. The energy stored follows the same pattern as above for this relationship but with the opposite variables, flow switched for effort and momentum for displacement.

## 5.3 Pseudo-Bond Graphs for Thermodynamic Modeling

As the name suggests, a pseudo-bond graph follows the general idea of modeling with bond graphs but with some differences. While the unifying convention for bond graphs is typically for power bonds to represent effort and flow variables that multiply to give power transferred between elements, the effort and flow variables in pseudo-bond graphs do not necessarily fit this requirement. The effort variable for a thermofluid system is temperature and the flow variable is heat flow, which has the same units as power. For the fuel injector model developed for this thesis, parallel power bonds connect each element, the top one repre-

senting conservation of mass with the effort and flow variables and pressure and mass flow, and the lower one representing conservation of energy showing the transfer of temperature ( $T$ ) and heat flow( $\dot{E}$ )

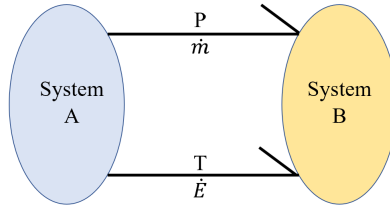


Figure 10: Pseudo-Bond Graph Variables

## 5.4 Injector Interior: Control Volume Modeling

The cylindrical volumes within the fuel injector models studied in this thesis are of particular interest, especially considering the gas dynamics and oscillations that may occur within these pipes. Each of these pipe sections is modeled using the technique developed by Kurt Strand ([Strand \(1991\)](#)). The basis of this modeling technique is in the conservation equations for 1-dimensional flow through constant cross-sections.

$$\frac{dU}{dt} + \frac{dE}{dx} = 0 \quad (5.9)$$

Where  $U$  and  $E$  represent the vectors for conservation of mass, momentum, and energy:

$$U = \begin{bmatrix} \rho \\ \rho u \\ \rho E \end{bmatrix} \quad \text{and} \quad E = \begin{bmatrix} \rho u \\ \rho u^2 + p \\ \rho H u \end{bmatrix}$$

Assuming 1-dimensional flow through constant-area ( $A$ ) channels of length " $L$ ," the full conservation equations that build the foundation of the sub-models for these portions of the fuel injector are:

$$A \frac{\partial}{\partial t} \int_0^L \rho dx = (\rho u A)_{x=0} - (\rho u A)_{x=L} \quad (5.10)$$

$$A \frac{\partial}{\partial t} \int_0^L \rho u dx = (\rho u^2 A + P A)_{x=0} - (\rho u^2 A + P A)_{x=L} - \int_0^L \pi D \tau dx \quad (5.11)$$

$$A \frac{\partial}{\partial t} \int_0^L \rho \left( e + \frac{1}{2} u^2 \right) dx = [\rho u A \left( h + \frac{1}{2} u^2 \right)]_{x=0} - [\rho u A \left( h + \frac{1}{2} u^2 \right)]_{x=L} - A \int_0^L \rho \dot{q} dx \quad (5.12)$$

Where:

$\rho$  = fluid density

$u$  = fluid velocity

$e$  = specific internal energy

$\tau$  = frictional shear stress tensor

$\dot{q}$  = rate of heat added per unit mass

$h = e + P/\rho$  = specific enthalpy

The integral equations stated above must be transformed into state space form for use in the bond graph model and subsequent flow simulation. The first step to this end is to divide the sections into a finite number of control volumes, from 1 to  $N$ , indexed by  $i$ . For a given number of control volumes, the size of each cell,  $dx$  is found by dividing the total length by the number of cells,  $dx = L/N$ . The convention for dividing the total volume into cells is shown in the image below.

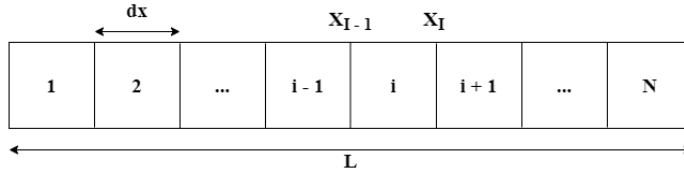


Figure 11: Control Volume Indexing Convention

It should be noted that the index notation uses lower-case letters for cell center values and upper-case letters for cell face values. Within each control volume, the properties in the state vector are assumed to be constant. This assumption reduces the number of independent variables to just one: time. The integral-form conservation equations can then be re-written to equations that replace the partial derivative with respect to time with the full derivative. Furthermore, the index notation on the right hand side of the following equations uses capital "I" rather than lower-case "i" to indicate the values are taken at the cell faces rather than the cell averages.

$$\frac{d}{dt}m_i = (\rho u A)_{x_{I-1}} - (\rho u A)_{x_I} \quad (5.13)$$

$$\frac{d}{dt}(mu)_i = (\rho u^2 A + PA)_{x_{I-1}} - (\rho u^2 A + PA)_{x_I} - \frac{\lambda}{2D} \rho_i u_i |u_i| A \Delta x \quad (5.14)$$

$$\frac{d}{dt}[m(e + \frac{1}{2}u^2)]_i = [\rho u A(h + \frac{1}{2}u^2)]_{x_{I-1}} - [\rho u A(h + \frac{1}{2}u^2)]_{x_I} + \dot{Q}_i \quad (5.15)$$

Where:

$m_i$  = total mass in control volume i

$\dot{Q}_i$  = total rate of heat added to control volume i

In order to produce the desired state vector of mass, momentum, and energy, the equations can be reordered once more to give the following, where momentum ( $mu$ ) is replaced with the variable  $p$  and the energy term [ $m(e + 1/2u^2)$ ] is replaced with the variable  $E$  to give the three equations that represent the model for dynamic fluid flow in a single control volume.

$$\frac{d}{dt}m_i = m_{I-1} - \dot{m}_I \quad (5.16)$$

$$\frac{d}{dt}p_i = m_{I-1}u_{I-1} + P_{I-1}A - \dot{m}_I u_I - P_I A - \frac{\lambda}{2D}m_i u_i |u_i| \quad (5.17)$$

$$\frac{d}{dt}E_i = m_{I-1}(h_{I-1} + \frac{1}{2}u_{I-1}^2) - \dot{m}_I(h_I + \frac{1}{2}u_I^2) - \dot{Q}_i \quad (5.18)$$

These equations together make up the state vectors for each of the control volumes within the pipe models at each time step. This method and the associated equations were developed by Kurt Strand for application to similar models to those used in this thesis ([Strand \(1991\)](#)). Additions to the model and tuning for accuracy were completed with the assistance of Professor Eilif Pedersen, who was also the primary developer of the boundary layer calculations. The model is coded such that flow in either direction is permitted and either isentropic or adiabatic conditions may be assumed. The complete code for one of the pipe models can be found in [Appendix B](#).



---

## 6 Methods

The bond graph method forms the theoretical basis for this design review through computer model simulation of a high pressure gas fuel injector. Existing formulations for fluid flow in pipes in the form of 20-Sim models were adapted into two different models that represent two iterations of the fuel injector's design. First, a simple model was evaluated for performance and flow properties both in the originally presented condition and after making slight adjustments to the internal geometry. When the manufacturer presented a more advanced version of the fuel injector, a new model was created to simulate the more complex arrangement and determine if and how it differed from the simpler version.

The motivation for this thesis is the investigation of how the current injector formulation performs as compared to when the dimensions of internal volumes are adjusted. As the design process progresses, it is essential to understand how performance can be affected as these sizes change. There are many considerations when choosing the internal sizing for such an essential engine component. These may include space constraints in the cylinder head, assurance of adequate flow through the many restrictions gas must pass through, and manufacturability given the current state of machine technology.

The following chapters step through the simulation of several injection cycles through the two models at a logical progression of different internal sizes. The importance of each of these changes is addressed immediately and recommendations made for how designers should consider the results. Additionally, some

of the guiding assumptions for this simulation are addressed and should serve to simplify models recreated in other software programs as the need arises.

---

## 7 Building the Simplified Model

Creating an accurate model of the simple high pressure gas fuel injector prototype allows for simulation of natural gas fuel flow dynamics during various engine operating conditions. Using the bond graph method in the 20-Sim software program facilitates the modification and combination of several existing and proven sub-models into an adequate representation of the high pressure fuel injector modeled for this thesis. The general arrangement of the first and most simplified fuel injector to be modeled is shown in the image below.

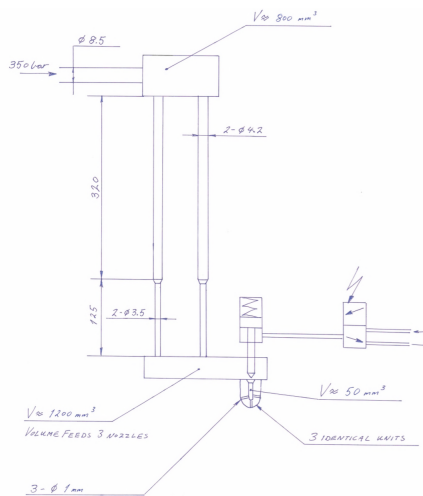


Figure 12: Simplified Sketch of Internals of the L'Orange Prototype High Pressure Gas Fuel Injector

Pressure waves during fuel injection in the two vertical supply volumes of the injector were studied as a part of a previous project and the sub-models for

these components originate from models created by Kurt Strand for his paper *Bond Graph Interpretation of One-dimensional Fluid Flow* ([Strand \(1991\)](#)). In the model, each volume is divided into control volumes with unique state vectors that are calculated iteratively during the simulation.

## 7.1 Boundary Conditions

The initial upstream conditions are assumed to be gas at 350 bar and 158° C, an assumption simplifying the supply line from the fuel storage tank. An extension of this project involves the modeling of gas dynamics in this supply line, so the injector model developed for this thesis will supplement the study of the system as a whole.

The downstream conditions after the fuel injector in the cylinder are modeled as an effort source (**Se**) with variable pressure and constant temperature. The temperature is constant and does not affect the flow and pressure modeling inside the injector, assuming all flow is one-way into the cylinder. The variable pressure was modeled based on in-cylinder measurements from a 4-stroke diesel engine with a maximum pressure of 120 bar. The shape of the pressure variation curve exhibits the characteristics of a typical rate of heat release (ROHR) curve, including a rapid rise in pressure for the first few degrees followed by a more shallow rise to the peak pressure and constant decrease as expansion concludes. This general curve shape was scaled vertically for different maximum pressures and horizontally for different engine speeds as needed for the simulations. The ratio of gas injection pressure to peak cylinder pressure was chosen to exceed 2 in order to avoid sub-critical gas flow during injection that may result in uneven mass flow [Senghaas \(2019\)](#).

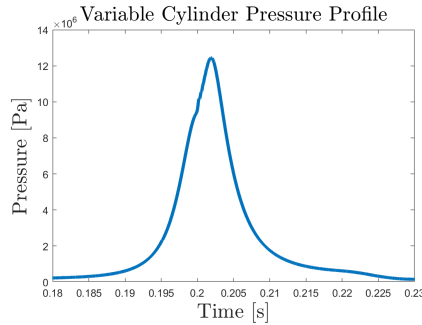


Figure 13: Variable Pressure Profile for Se Element

## 7.2 Valves

The vaporized fuel in the injection ports is treated as an ideal gas so that mass flow, pressure, and temperature dynamics can be modeled using the isentropic nozzle equation.

$$\dot{m} = A \frac{P_u}{\sqrt{T_u}} \sqrt{\frac{2\kappa}{R(\kappa-1)}} \sqrt{P_r^{2/\kappa} - P_r^{(\kappa+1)/\kappa}} \quad (7.1)$$

Where:

$$P_r = \begin{cases} \frac{P_{out}}{P_{in}}, & \text{for } \frac{P_{out}}{P_{in}} > P_{crit} \\ P_{crit} & \text{for } \frac{P_{out}}{P_{in}} \leq P_{crit} \end{cases}$$

$$P_{crit} = \left( \frac{2}{\kappa + 1} \right)^{\kappa/(\kappa-1)} \quad (7.2)$$

These equations are coded into the modulated resistor (**MR**) component of the bond graph. The modulated part of this component is the variable valve area that models the changing flow area available as the pin retracts and allows fuel to flow

into the cylinder. The boundary conditions on either side of the valve as well as the valve area and opening profile determine the mass flow into the cylinder.

### 7.3 Cylindrical Volumes

The upper and lower portions of the connection between the gas supply and the ring volume that houses the injector needles are modeled as cylindrical "pipes" with a small tapered section connecting them. These volumes are where any pressure waves that result from the high-pressure injection to occur, so the technique to model them must facilitate study of the pressure and flow dynamics within the slender volumes.

### 7.4 Simple 20-Sim Model

This first iteration of a simplified injector model for the first design provided was assembled in 20-Sim and appears in the image below.

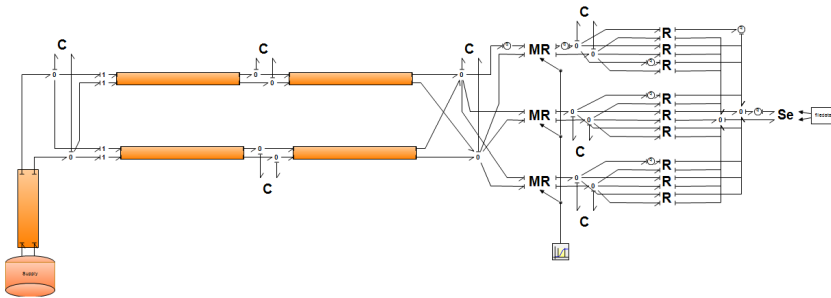


Figure 14: Simple Injector Model

The two parallel pipes with different diameters feed the three needles represented by MR elements. The needles are actuated by a simple ramp profile for a normal operating speed of 600 RPM. The nine R elements represent the ports

into the cylinder, which has variable pressure as previously described supplied by an external file to the **Se** element.



---

## 8 Initial Parameters and Assumptions

The bond graph model of this high pressure gas fuel injector is intended to simulate the pressure and flow variations that occur during normal, steady operation of the engine. A prototype of the modeled injector will be tested in a single-cylinder test engine soon, but until that is possible the working properties of that engine will be approximated for the simulations that comprise this project. These working properties include a normal operating speed of 600 RPM and a maximum cylinder pressure of 120 bar.

### 8.1 System Initial Conditions

The initial conditions in the system are based on the assumption of an upstream methane supply pressure of 350 bar and at a temperature of  $-115^{\circ}\text{C}$  (158 K). While the true composition of LNG has additional components, the starting point for all simulations used these simplified assumptions to isolate how changes in injector geometry impacted pressure and mass flow. Additional models for the pipe system upstream of the injector model used in the simulations are in development to provide a complete picture of how many more factors can affect the pressure and mass flow variations in this novel injector design. The boundary condition at the injector exit is the variable cylinder pressure profile discussed previously.

## 8.2 Injection Profile

The duration of injection was chosen starting with the assumption that this system will be hydraulically actuated by a cam and thus injection will occur over the same number of crank degrees for any speed. Manufacturer estimates for the high pressure gas injector to be modeled indicate that injection duration should take place over approximately  $22^\circ$ , which translates to 4 milliseconds at 600 RPM. The shape of the injection profile was chosen to reflect a single motion of the injector needle, up then down. Many options exist for refining the shape of the injection profile, but a sine wave was selected in order to account for delays and inertia effects due to hydraulic actuation of the needle. This profile was applied to the model through the modulated resistor (MR) components which simulate needle motion. The ramp from closed to open on the profile occurs over 0.1 millisecond on either side.

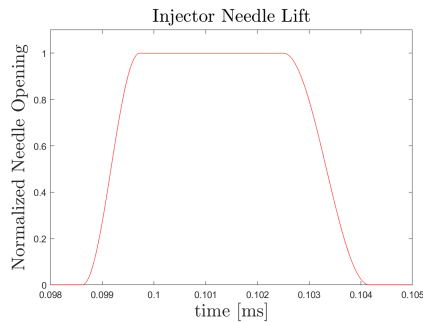


Figure 15: Motion Profile for Injector Needle Opening

### 8.3 Heat Transfer

The model assumes that no heat transfer occurs between the internal surfaces of the injector and the gas as it rapidly moves through each space and into the cylinder. This assumption was evaluated for accuracy by creating a very simple model of a single pipe and gas flowing from a high-pressure reservoir on one side to a low-pressure reservoir on the other side. While the exact oscillations observed in the pipes were not approximated by this simplification, the velocity was closely replicated.



Figure 16: Simple Pipe Model for Heat Transfer Investigation

The maximum gas velocity observed in the middle of one of the pipe sections in the full injector model during injection was 172 m/s. This velocity was achieved in the simplified model by setting the high pressure reservoir to 350 bar and the low pressure reservoir to 330 bar. A constant interior wall temperature was assumed to be 393 K which corresponds to a temperature of approximately 100 K above ambient conditions.

Heat transfer from the walls to the gas was modeled as energy addition to the final element of each control volume's state vector. The formula for the calculation of total energy in the control volume with this addition is shown below.

$$\text{Energy}[i] = \text{Cell Face Energy}[i] - \text{Cell Face Energy}[i+1] - \alpha \times A_{\text{pipe}} \times (T_{CV_i} - T_{\text{wall}}) \quad (8.1)$$

Where:  $\alpha$  = Thermal Diffusivity

$A_{pipe}$  = Internal Pipe Surface Area

$T_{CV_i}$  = Temperature of Control Volume "i"

$T_{wall}$  = Wall Temperature

The value for thermal diffusivity was solved for by setting two established equations for the Nusselt Number (Nu) equal to each other. This produced an equation where  $\alpha$  exists only as a function of gas velocity  $U$ . The two equations for the Nusselt Number are shown below:

$$Nu = \frac{\alpha \times L}{\lambda} \quad (8.2)$$

$$Nu = 0.027 \times Re^{4/5} \times Pr^{1/3} \times \left( \frac{\mu}{\mu_s} \right)^{0.14} \quad (8.3)$$

Where:  $L$  = Characteristic Length (diameter for pipes) [m]

$\lambda$  = Thermal Conductivity [W/(m-K)]

$Re$  = Reynolds Number [-]

$Pr$  = Prandtl Number [-]

$\mu$  = Fluid Dynamic Viscosity at Average Temperature [Pa-s]

$\mu_s$  = Fluid Dynamic Viscosity at Wall Temperature [Pa-s]

The ratio of dynamic viscosities is very close to unity and is assumed to be constant at 1 for the rest of the calculations. The formulas used for the Reynolds and Prandtl numbers were:

$$Re = \frac{U \times diam \times \rho}{\mu} \quad (8.4)$$

$$Pr = \frac{\mu \times C_p}{\lambda} \quad (8.5)$$

Where:  $U$  = Gas velocity [m/s]  $\rho$  = Gas density [kg/m<sup>3</sup>]

Combining these equations to solve for  $\alpha$  as a function of gas velocity  $U$  gives:

$$\alpha(U) = \frac{\lambda}{diam} \times 0.027 \times U^{4/5} \times \left( \frac{diam \times \rho}{\mu} \right)^{4/5} \times \left( \frac{\mu \times C_p}{\lambda} \right)^{1/3} \quad (8.6)$$

The expected unit for  $\alpha$  is  $\frac{W}{m^2K}$  which is the same unit that results from the first term  $\frac{\lambda}{diam}$  which is also the only term in the equation that is not non-dimensional. Because all values in the equation are considered constant except for the velocity, a single coefficient can be calculated for use in the model to estimate the effect of heat transfer from the pipe. The simplified equation for  $\alpha$  is:

$$\alpha(U) = 211.9 \times U^{4/5} \quad (8.7)$$

<b>Term</b>	<b>Value</b>
$\mu$	$2.4 \times 10^{-5} \text{ kg/m} \cdot \text{s}$
$\rho$	$190 \text{ kg/m}^3$
$C_p$	$3.158 \text{ J/kg} \cdot \text{K}$
$\lambda$	$0.0765 \text{ W/m} \cdot \text{K}$
$diam$	$0.0034 \text{ m}$

Table 1: Input Values for  $\alpha(U)$  Calculation

The relationship between  $\alpha$  and gas velocity,  $U$ , is shown in the image below.

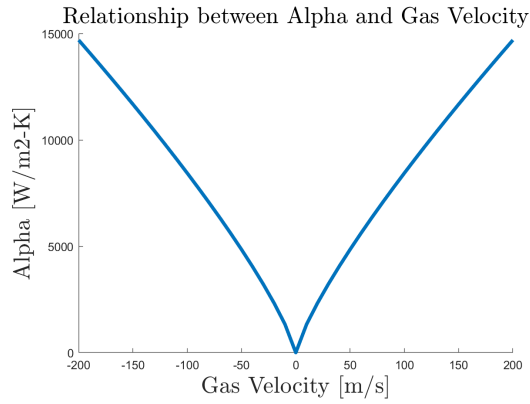


Figure 17: Heat transfer coefficient for a range of gas velocities

When the modification to the energy equation described in equation 8.1 was included in the simulation, the temperatures calculated for the control volumes between the pipe ends saw a slight increase in temperature, shown in the image below.

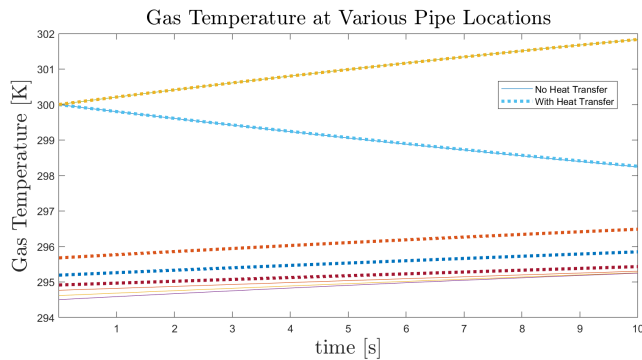


Figure 18: Comparison of Temperatures with and without Heat Transfer in Pipe

This investigation and demonstration of minimal temperature rise is sufficient to conclude that adiabatic conditions may be assumed for the larger model since

adding heat transfer to the equations does not change the gas temperature by enough to justify the additional simulation time required. This is likely due to the fact that the gas moves sufficiently fast through the pipe and the temperature difference is not large enough to have an impact in the simulations.

## 8.4 Loss Coefficients

Selection of either adiabatic or isentropic conditions occurs in the model through the loss coefficients labeled "xflM" and "xflP" for the left and right end of the pipe, respectively. If this parameter is negative, isentropic conditions are assumed. Otherwise, adiabatic conditions are assumed.

### 8.4.1 Isentropic Conditions

If isentropic flow is assumed, the pressure in the first control volume is determined by the general thermodynamic relationship between pressure and temperature shown in the equation below.

$$\frac{P}{P_1} = \left( \frac{T}{T_1} \right)^{\frac{\kappa}{\kappa-1}} \quad (8.8)$$

The pressure in the first control volume is originally determined by upstream conditions but must be corrected using the isentropic flow equation. The upstream conditions in the equation are indicated by the variables  $T_1$  and  $P_1$  and the corrected variables are  $T$  and  $P$ . The temperature used in the numerator on the right hand side of equation 8.8 comes from an adjustment described in the equation below.

$$T = T_1 - tfactlM \times \frac{(u[2])^2}{2 \times C_p} \quad (8.9)$$

This correction is necessary to correct the stagnation temperature set from the inlet conditions,  $T_1$ , to the real temperature  $T$  in order to calculate the constants and flux values required to establish the states in every control volume. The variable  $t_{factLM}$  is a loss coefficient to decide the degree to which the isentropic correction for dynamic temperature rise is used in the temperature correction equation. When this value is 1, full isentropic conditions are assumed but as it is reduced, a temperature closer to the stagnation temperature is used in the calculations. The influence of changing this parameter on the flow in the simplified pipe model was investigated to produce the figures below for comparison.

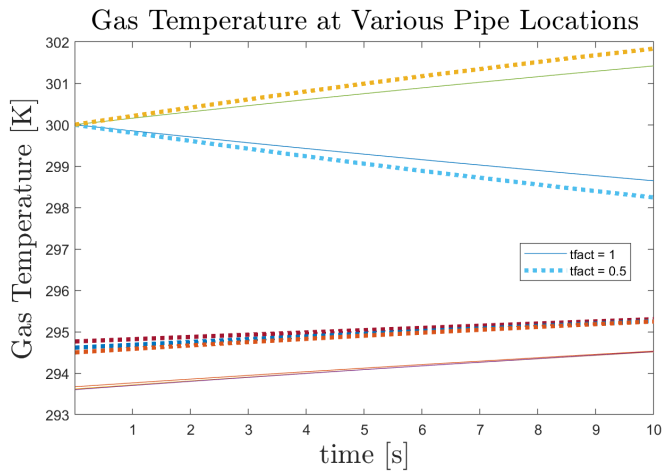


Figure 19: Comparison of Temperatures different  $t_{fact}$  Parameter Values

The most significant difference observed with the  $t_{factLM}$  parameter is changed from 0.5 to 1 is that the the temperature at the interior pipe locations are slightly lower. This is reasonable considering equation 8.9 where the correction for dynamic temperature rise is doubled when  $t_{factLM}$  is changed from 0.5 to 1, thus making the calculated temperature slightly smaller. In general, the temperature

differences observed in this simplified model are not significant enough to give rise to any concern about the assumption of isentropic conditions being assumed for the flow through all the pipe elements in the model.

### 8.4.2 Adiabatic Conditions

Assuming the gas exchanges no heat with the environment as it flows through the injector and into the piston allowed for many simplifications in the earlier model. Assuming no heat transfer from internal injector surfaces has already been proven reasonable, but when adiabatic conditions are chosen in the pipe model rather than isentropic, pressure and temperature calculations change. When the parameter  $xflM$  is positive, it becomes an element of the pressure calculation used instead of the equation for isentropic assumptions, equation 8.8.

$$P = \frac{P_1}{1 + red} \quad (8.10)$$

$$red = \frac{xflM \times (u[1])^2}{R \times T} \quad (8.11)$$

Where  $T$  is calculated as described in equation 8.9. Similar to how stagnation temperature was found using the dynamic temperature, for the adiabatic calculations, dynamic pressure must be used to correct the pressure. The dynamic pressure correction is shown below

$$q = \frac{\rho \times (u[1])^2}{2} \quad (8.12)$$

The reduction factor  $red$  includes the scaling parameter  $xflM$  to adjust the effects of this correction on the system. The result of adjusting the scaling param-

eter on the pressure and temperature observed in the simplified pipe model are shown in the images below.

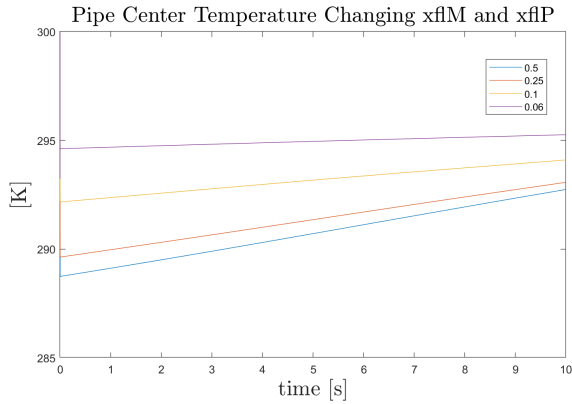


Figure 20: Temperature Effects of Changing Adiabatic Scaling Parameter

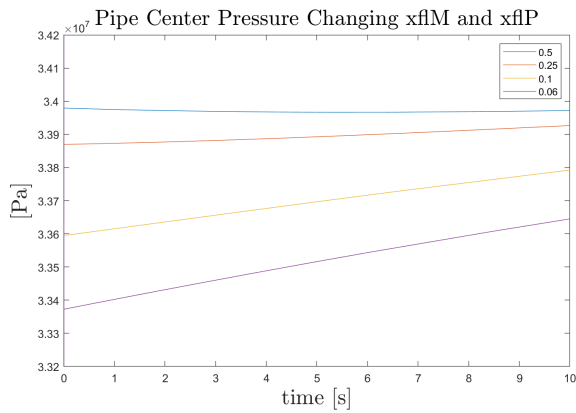


Figure 21: Pressure Effects of Changing Adiabatic Scaling Parameter

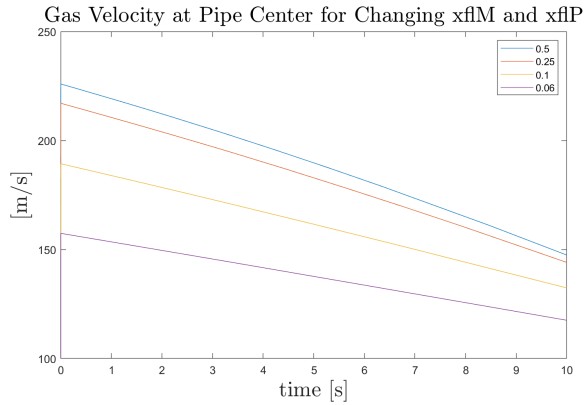


Figure 22: Velocity Effects of Changing Adiabatic Scaling Parameter

As expected from the pressure correction equation, increasing the  $x_{flM}$  parameter decreases the pressure and thus temperature is increased.

### 8.4.3 Concluding Remarks

The result of these investigations is that adiabatic and isentropic conditions may be assumed for this model. The model verification investigations conducted in this thesis are some of the first conducted for this fuel injector. Later, as the design is fine-tuned, it would be useful to re-evaluate these assumptions and verify their accuracy with a physical prototype.



---

## 9 Testing the Simplified Model

The driving force for mass flow of fuel through the injector is the high gas pressure upstream. Larger volumes inside the injector, relative to the volume of gas injected per cycle, allow for a greater buffer against the negative consequences of restricted and insufficient fuel flow. The overall injector size is limited, but it is of interest to investigate how changing each of the internal volumes affects the mass flow into the cylinder and the pressure variations in the final volume before injection.

For clarity, the vertical cylindrical volumes connecting the upper volume fed by the supply line to the lower ring volume that houses the injector pins will be called "pipes" from this point forward.

### 9.1 Parameter Sweep Simulations

The variation in parameters for this investigation includes a 20% and 40% increase and decrease for each, and simulations were run for every combination of these changes and compared to understand where any significant differences exist. A summary of these parameters as well as the original values provided are shown in the table below and a complete list of the input parameters for the simulation can be found in [Appendix A](#).

	Change From Original Values	Upper Volume (V4)	Twin Vertical Pipes (V23)		Ring Volume (V1)	
		Volume [mm <sup>3</sup> ]	Volume [mm <sup>3</sup> ]	Upper Pipe Diameter [mm]	Lower Pipe Diameter [mm]	Volume [mm <sup>3</sup> ]
1	-40%	522	3380	3.261	2.69	720
2	-20%	696	4510	3.766	3.107	960
3	Original Value	870	5640	4.21	3.473	1200
4	+20%	1040	6770	4.612	3.805	1440
5	+40%	1220	7900	4.982	4.11	1680

Table 2: Internal Volume and Diameter Changes for Initial Model Simulations

The first observation from the results of the several parameter sweep experiments performed is that changing the upper volume, V4, while keeping the other volumes constant has a minimal effect on the mass flow into the cylinder and pressure variation in the ring volume, V1. This is likely because the volume ranges chosen are all sufficiently large to provide an adequate pressure source to drive the flow throughout the system. The design implication for the fact that few changes were seen in the data for these significant volume adjustments is that volume V4 can be altered as needed for space constraints with minimal concern for changing injector performance.

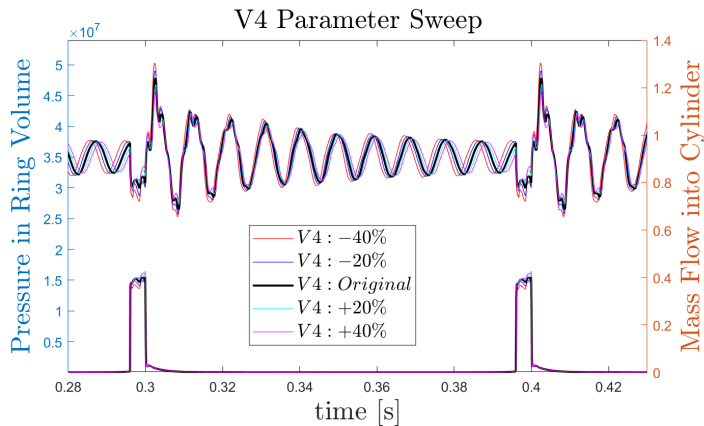


Figure 23: Parameter Sweep Results for Upper Volume (V4)

For a constant ring and upper volume ( $V_1$  and  $V_4$ ), changing the pipe volume ( $V_{23}$ ) is more likely to change the mass flow and pressure variations in the injector since the total volume injected per cycle includes some fuel stored in the pipes. The image below illustrates the approximate volume occupied by the fuel injected during one cycle, assuming ideal gas conditions to determine the volume at 350 bar occupied by the measured mass flow into the cylinder. The gray shading indicates the 0.0017 kg injected per cycle which occupies approximately 3,900 cubic millimeters within the injector.

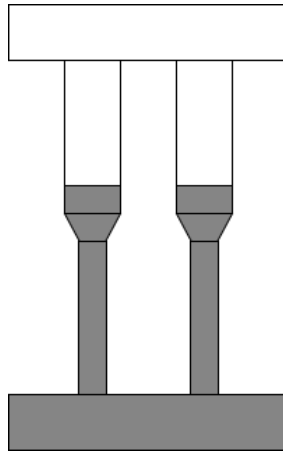


Figure 24: Approximate Representation of Volume Injected per Cycle

Understanding that a large portion of injected gas comes from the pipes explains the significant differences seen in pressure and mass flow for the parameter sweep experiment.

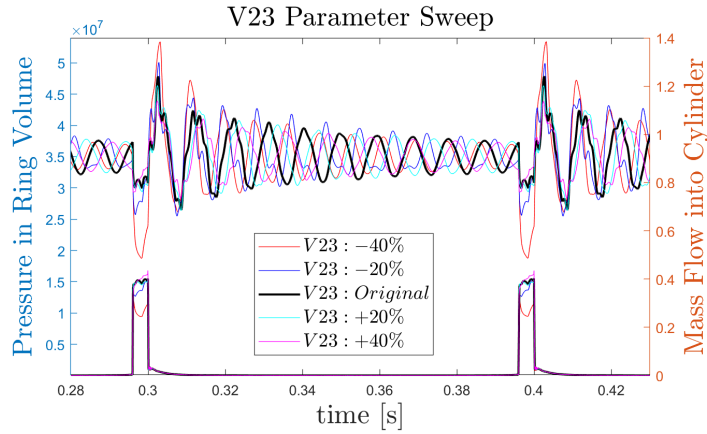


Figure 25: Parameter Sweep Results for Pipe Volume (V23)

These results imply that pipe volume is a significant consideration during design of this injector. If the pipes require re-sizing for volume constraints, simulations and physical tests must be carried out to ensure the new arrangement does not significantly alter injector performance.

Changing the ring volume (V1) had little impact on the pressure and mass flow data gathered from the parameter sweep experiment. The volume of fuel injected exceeds the value of each volume iteration of V1. If V1 were to be larger than the volume injected, some change in the results may be possible. Sizing this component so much larger is very unlikely, however, and changing the pipe volumes will always have a greater impact on injector performance than changing the ring volume.

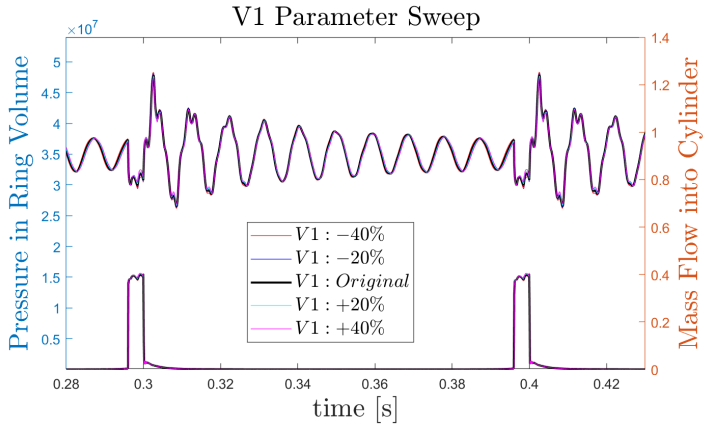


Figure 26: Parameter Sweep Results for Ring Volume (V1)

For a better comparison of these three parameter sweep experiments, the time around injection is magnified in the following three images.

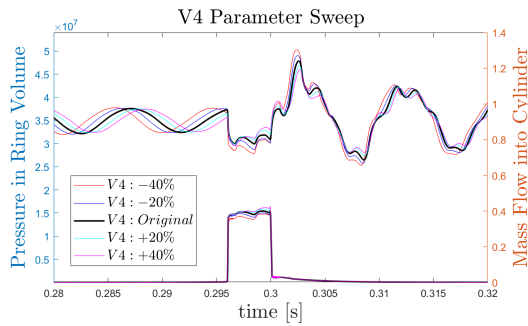


Figure 27: Upper Volume (V4)

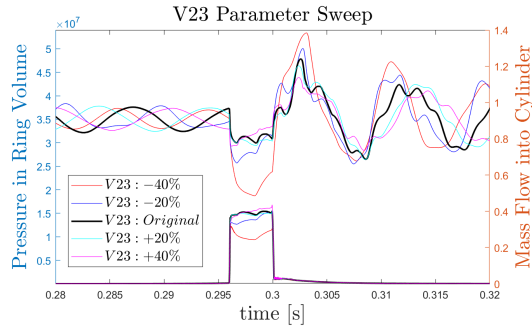


Figure 28: Pipe Volume (V23)

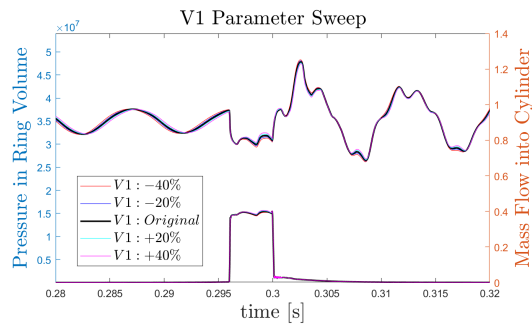


Figure 29: Ring Volume (V1)

## 9.2 Pressure Waves

The significant differences observed in the pressure fluctuations for the pipe volume parameter sweep require a closer investigation into their characteristics and implications.

The following figures show side-by-side comparisons of the ring volume pressure for original pipe volume and three progressively smaller values.

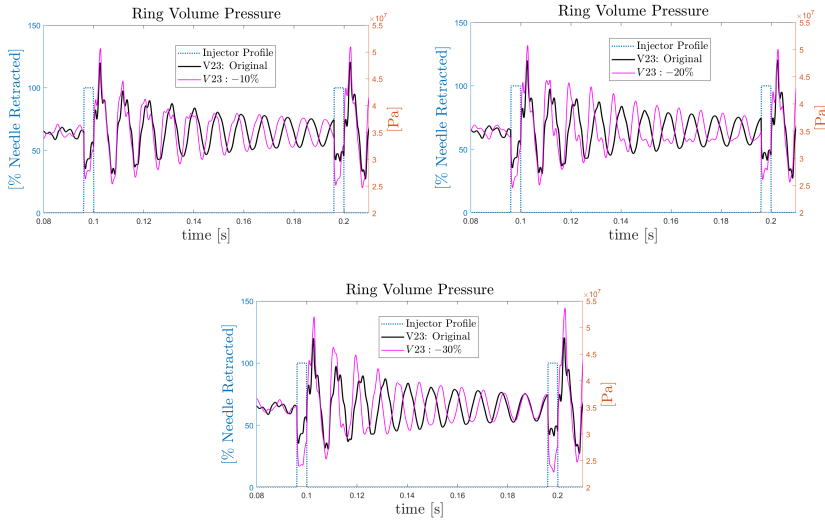


Figure 30: Ring Volume Pressure for Decreasing Pipe Diameter

This data illustrates how decreasing the volume of the pipes results in a slight increase in pressure wave frequency and amplitude. It was assumed that frequency was tied to pipe length, but the plot showing a comparison of the pressure waves between the original volume and the 30% decreased volume shows one additional peak in the injection interval, approximately increasing the frequency from 110 Hz to 120 Hz. This indicates that pipe volume, not length, has an effect on pressure wave frequency between injections.

Increasing the pipe diameter by the same increments produces a decrease in both pressure wave frequency and amplitude, showing in Figure 31 below.

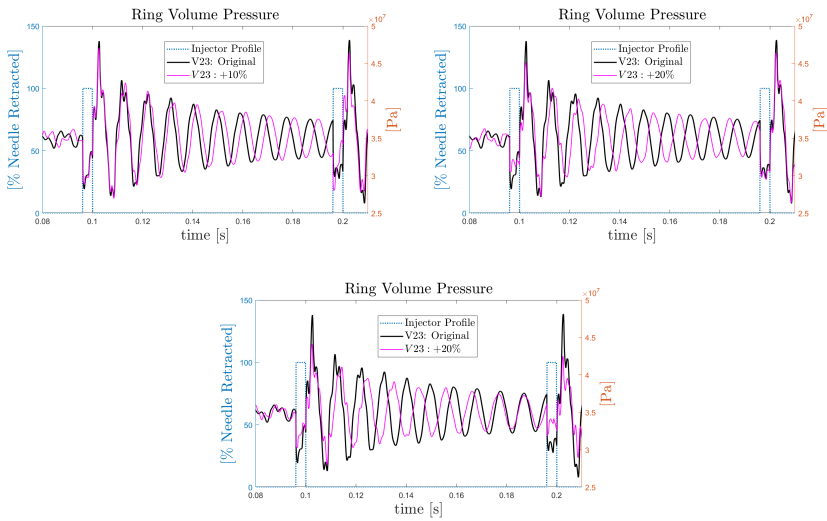


Figure 31: Ring Volume Pressure for Increasing Pipe Diameter

While it was initially assumed that the frequency of pressure oscillations in the system depended on the length of the pipe and the associated harmonics, this brief investigation reveals there may be a different driving force for the oscillations. The pressure waves inside the pipes appear to be very similar to those observed in the rest of the system, with close to equivalent pressures throughout the pipe rather than waves of different pressures moving through the pipes in the time between injections. The image below illustrates how the dominating pressure fluctuations are more connected to the frequency observed throughout the system rather than the pressure differences observed in the pipe alone. In other words, the pressure in the pipe remains consistent and fluctuates together with the same frequency as is observed in the rest of the system.

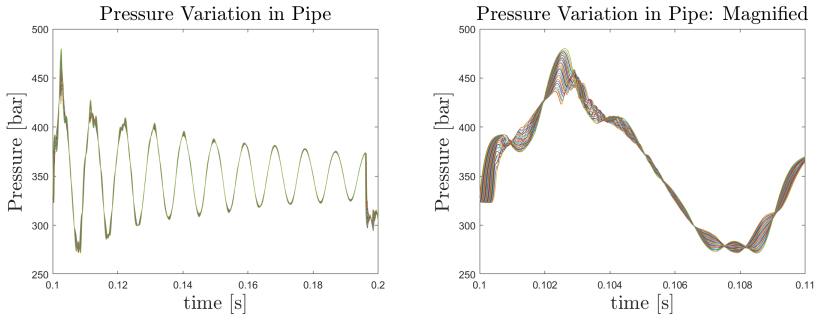


Figure 32: Pressure Variation Within Pipe

The zoomed-in image on the right shows the pressures in each individual control volume within one pipe. The fact that they are so tightly grouped indicates that the pipe is close to constant pressure throughout the cycle and the dominating frequency of pressure oscillation is that frequency which dominates throughout the system, shown clearly in the zoomed-out image on the left. The frequency observed in the left image is 110 Hz, which is the same as the frequency of the oscillations observed in the rest of the system.

Previously, the effect of changing each volume on this dominating frequency was investigated and the pipe volume was concluded to have the biggest effect on the dominating frequency. This correlation is likely not due to the length or significant pressure waves developed as a result of this long, pipe-shaped volume, but rather due to the fact that the pipe volume accounts for a significant portion of the overall injector volume.

### 9.2.1 Pressure Drop During Injection

While the pressure waves are important to understand the gas dynamics inside the injector, the pressure drop in the ring volume during injection is important

to study as well, since pressure is the driving force for injection. The following images show how both decreasing and increasing the pipe volume changes the pressure drop during injection.

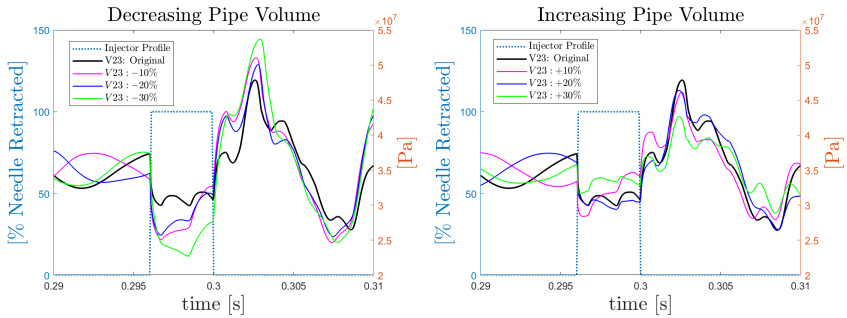


Figure 33: Pressure Drop During Injection for Changing Pipe Volume

Changing the ring and upper volumes also has an impact on the pressure drop during injection. The images below show that changing the ring volume has a smaller effect on the pressure drop than changing the upper volume.

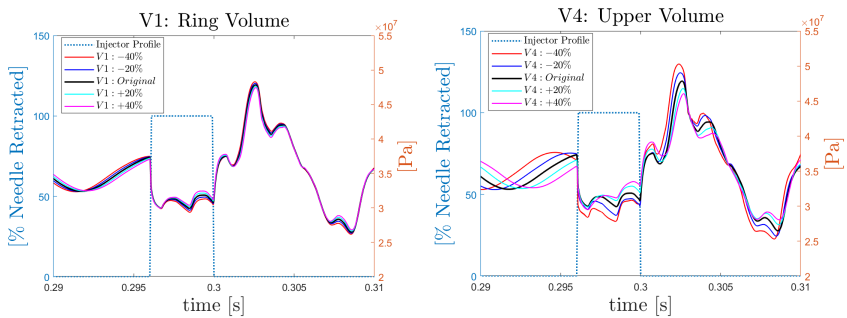


Figure 34: Pressure Drop During Injection for Changing Ring and Upper Volumes

---

## 10 Application to Advanced Model

As the injector design was refined by the manufacturer, a new schematic was provided and modeled using the principles and correlations investigated with the simplified model described in previous chapters. The new design adds several more channels than the simple pair of parallel pipes used for the old model. The gas travels through several branching paths to reach the same 3-pin injector arrangement at the cylinder that was modeled previously.

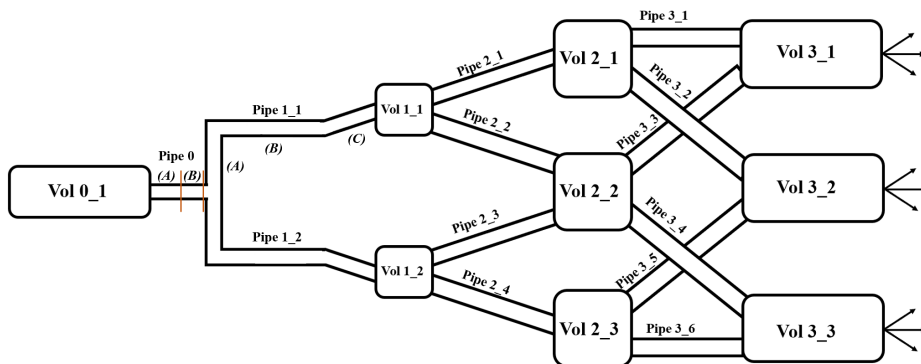


Figure 35: Simplified Graphic of Advanced Model

In the 20-Sim model, Pipe 0 A and B are represented by the elements "Pipe 0" and "Vol 0\_2", respectively. This decision was made for the functionality of the model since pipe elements cannot be modeled next to each other without a capacitor element (volume) in between. The small size of Pipe 0 B facilitates this adjustment.

<b>Component</b>		<b>Length [mm]</b>	<b>Diameter [mm]</b>	<b>Volume [mm<sup>3</sup>]</b>
<i>Vol 0_1</i>		-	-	91110
<i>Pipe 0</i>	A	101.6	4.78	1823.2
	B	8	5.2	169.9
<i>Pipe 1_1</i>	A	20	3.5	384.8
	B	60.7	3.4	1102.2
	C	14.7	3.4	266.9
<i>Vol 1_1</i>		10	4	251.3
<i>Pipe 2_1</i>		45.8	2.6	972.7
<i>Vol 2_1</i>		10.2	4.3	449.5
<i>Pipe 3_1</i>		26.2	2.6	834.6
<i>Vol 3_1</i>		15.2	2	143.3

Table 3: Internal Sizes for Advanced Injector Model

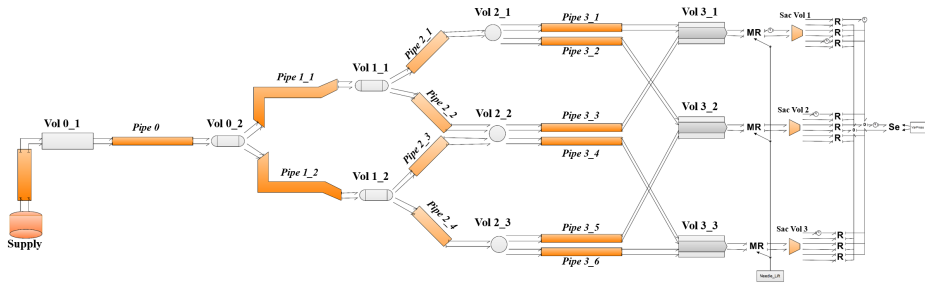


Figure 36: Advanced Model in 20-Sim

## 10.1 Internal Volumes

As the design of this fuel injector is refined, the size of each of the internal volumes may be adjusted as needed for space and flow concerns. The purpose of the following sections is to evaluate how changing each volume individually affects the mass flow of fuel into the cylinder. This property alone was isolated as the most important factor to consider when increasing or decreasing internal volumes. Since pressure is a driving force for fuel injection in this system, changing

the internal volume should proportionately change the mass flow of fuel. The size of the pipe elements were not varied for the advanced model in the same way they were for the simplified model described previously. It is assumed that the relationships and dynamics observed in the simplified model will be replicated in the advanced model.

The overall volume of the advanced model is smaller than the simple model. As such, the volume of gas injected per cycle makes up a much larger percentage of the overall internal volume than before. This amount is shown graphically in the image below.

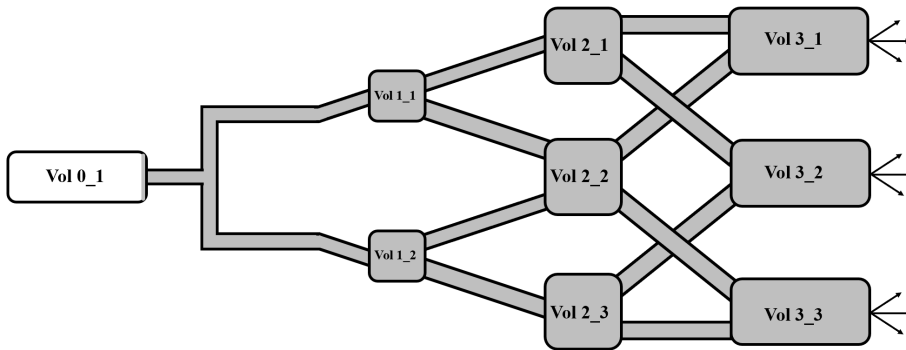


Figure 37: Fuel Injected Per Cycle Represented as a Percentage of Injector Volume

### 10.1.1 Variation in Top Volume

In the same way that volumes were changed in the simplified model to understand how each parameter changes injector performance, a similar analysis was conducted on the more advanced model. First the size of the volume (capacitor) elements was changed and the results analyzed, then the same procedure was repeated for the pipe volumes.

First, Vol 0\_1, the first volume gas enters from the supply line, was changed to understand how adjusting this parameter impacts overall performance. It was hypothesized that increasing this volume would provide a stronger driving force for fuel flow into the combustion chamber. Furthermore, it should help to dampen the effects of pressure variations caused by flow through the many restrictions in the injector. The first result investigated was the mass flow of fuel into the cylinder when the upper volume was increased and decreased by factors of 2 and 4. The results are shown below including the injector needle opening profile for reference.

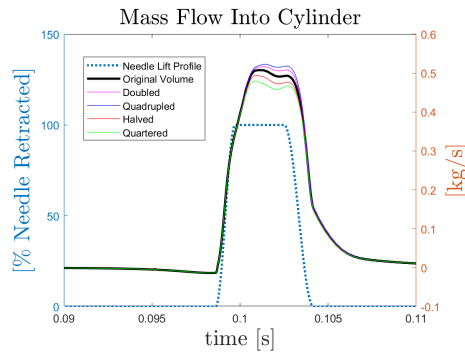


Figure 38: Mass Flow into Cylinder for Changing Volume 0\_1

The effect of any change in the top volume is slight but exists. This is a parameter that could be tuned for a desired increase or decrease in fuel mass flow into the cylinder. Next, the size of the smaller volume, Vol 0\_2, was changed by the same factors. Because this volume is so much smaller than Vol 0\_1, the effect of these changes on mass flow into the cylinder is also much smaller. The nearly imperceptible changes shown in the figure below indicate that Vol 0\_2 may be changed as space restrictions in the injector housing require.

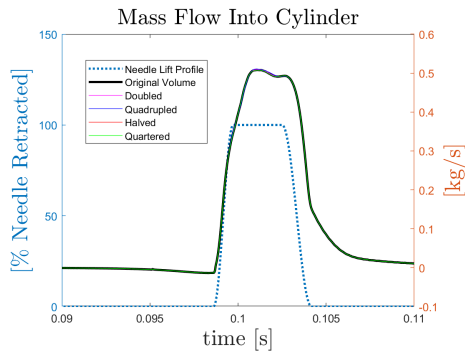


Figure 39: Mass Flow into Cylinder for Changing Volume 0\_2

### 10.1.2 Volume 1 Changes

The volumes labeled "Vol1\_1" and "Vol1\_2" in Figure 36 were changed by the same factors as Vol 0\_1 and Vol 0\_2. Because these spaces are already very small, these adjustments had minimal effect on the mass flow into the cylinder.

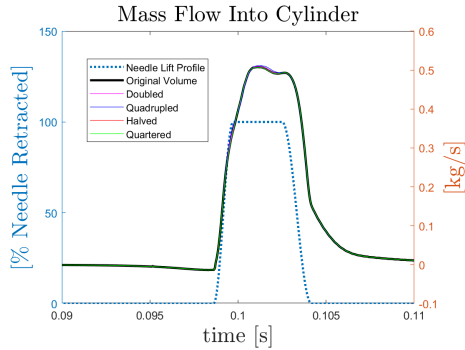


Figure 40: Mass Flow into Cylinder for Changing Volumes 1\_1 and 1\_2

The effect of changing these volumes is very similar to the effect of changing Vol 0\_2. If the injector had to be re-sized, changing this particular volume by the factors tested is estimated to have a minimal effect on the injection properties of

the device.

### 10.1.3 Volume 2 Changes

Similar results occur when Volumes 2\_1, 2\_2, and 2\_3 are changed by the same factors as Volumes 1\_1 and 1\_2, likely because the starting value for both sets of volumes are very similar. The difference in mass flow between volume adjustments is more apparent with this set of volumes than the previous trials. This is expected since there are three volumes being changed in this trial so the overall internal volume of the injector changes more than it did when Volume 1\_1 and 1\_2 were changed.

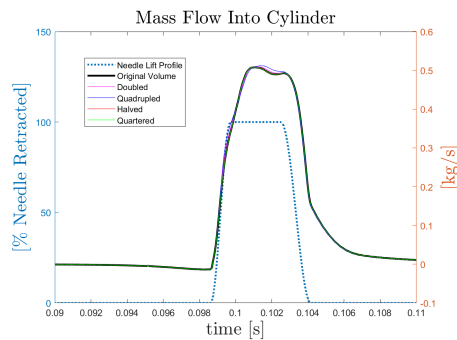


Figure 41: Mass Flow into Cylinder for Changing Volumes 2\_1, 2\_2, and 2\_3

### 10.1.4 Volume 3 Changes

The same trend continues as the final volume before the needles, Volumes 3\_1, 3\_2, and 3\_3, are changed by the same factors as the previous volumes.

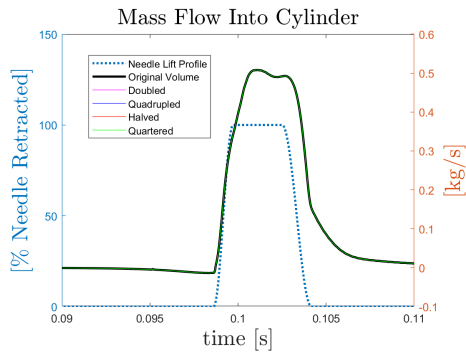


Figure 42: Mass Flow into Cylinder for Changing Volumes 3\_1, 3\_2, and 3\_3

### 10.1.5 Sac Volume Changes

The final volume modeled in 20-Sim is the sac volume. This area is constantly exposed to the cylinder conditions as it is the connecting area between the needle and the three injector ports before gas enters the cylinder.

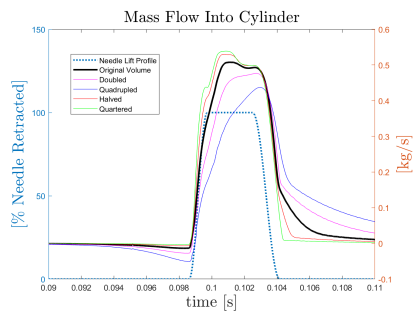


Figure 43: Mass Flow into Cylinder for Changing Sac Volumes

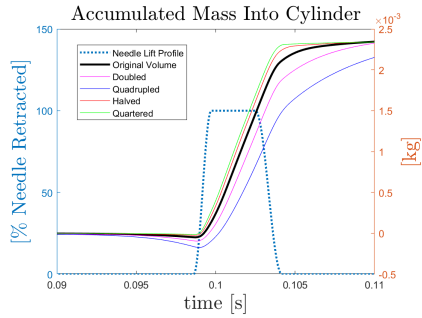


Figure 44: Mass per Injection for Changing Sac Volumes

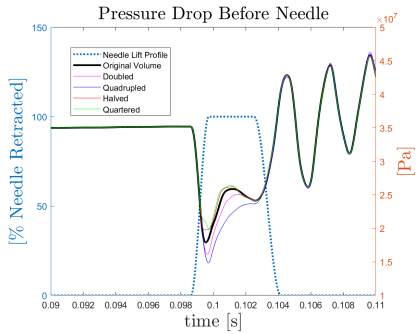


Figure 45: Pressure Drop Before Needle for Changing Sac Volumes

It is unlikely that any gas remaining in the sac volume would be burned during the engine's power stroke, so an increase in sac volume would also correspond to an increase in unburned fuel emissions. Reduction of harmful methane emissions is one of the goals of this new fuel injector design, so it logically follows that the smallest sac volume possible should be used. The limitations on this size include manufacturing abilities and size requirements for the three ports into the cylinder that aid in spray development and fuel/air mixing.

### 10.1.6 Top Valve Use

The option exists to use an alternative gas inlet valve. When this valve supplies gas to the injector, the effect is simplified in the model to be represented as an increase in the dimensions of the parallel pipes in the upper portion of the injector shown in Figure 36 as Pipe 1\_1 and Pipe 1\_2.

	<i>Original Value</i>	<i>Value When Upper Gas Inlet Used</i>
<i>Diameter [m]</i>	$3.4 \times 10^{-3}$	$5.1 \times 10^{-3}$
<i>Length [m]</i>	$9.54 \times 10^{-2}$	0.376

Table 4: Top Pipe Size Assumptions for Optional Top Valve Use

Increasing the volume of these pipes results in a slight increase in the mass of fuel injected per cycle, likely due to smaller fluctuations in pressure before the needle. A larger volume upstream of the injection port provides a greater buffer against pressure variations in the period between injections, driving the flow of gas into the cylinder at a more constant rate. These conclusions are summarized in the figures below.

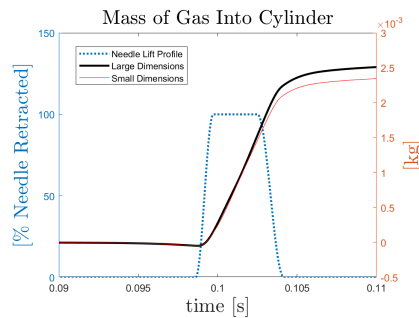


Figure 46: Slight Increase of Mass into Cylinder for Increasing Upper Pipe Size

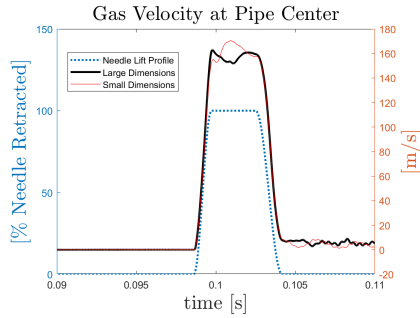


Figure 47: Similar Gas Velocity for Changing Upper Pipe Size

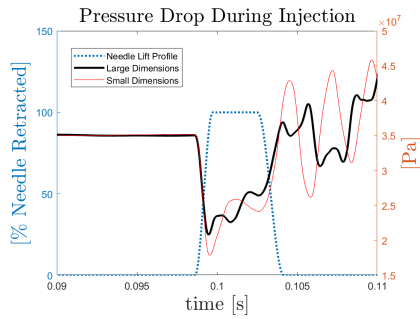


Figure 48: Slight Decrease in Pre-Needle Pressure Fluctuations for Changing Upper Pipe Size

## 10.2 Inlet Pressure

An upstream pressure of 350 bar has been assumed for all simulations so far. Reducing this pressure should produce a proportional reduction in mass flow and mass injected into the cylinder. This hypothesis was tested by reducing the upstream pressure from 350 bar to 200 bar by increments of 50 bar and the results are shown in the following images.

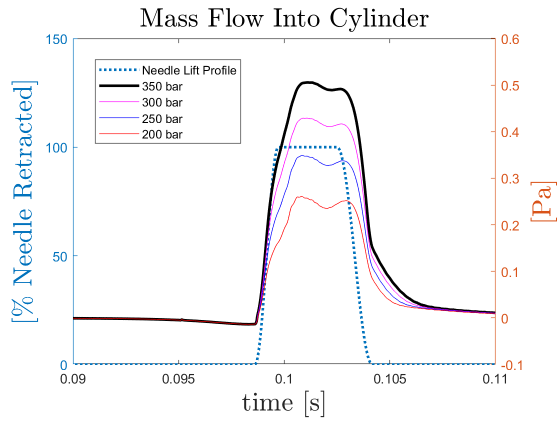


Figure 49: Mass Flow for Changing Initial Pressure

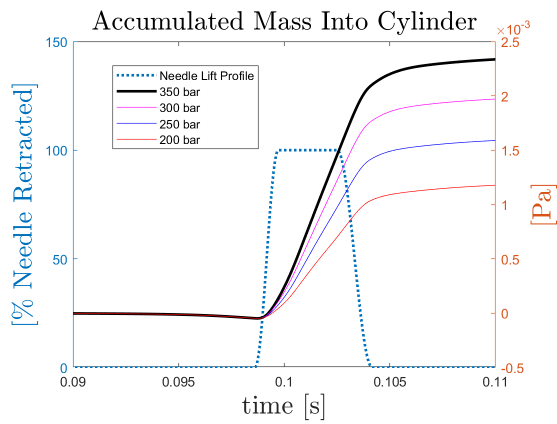


Figure 50: Mass Injected Per Cycle for Changing Initial Pressure

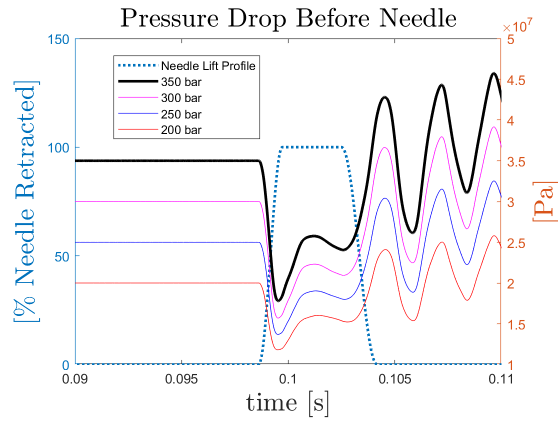


Figure 51: Pressure Drop During Injection for Changing Initial Pressure

As expected, the mass flow and mass injected per cycle decrease linearly with supply pressure. The pressure drop during injection in the pre-needle volume is not as significant for lower pressures. This is likely because as the upstream pressure decreases, it is closer to the downstream pressure from the cylinder so the drop during injection is less significant.

### 10.3 Injection Duration

The original duration of injection was 20 degrees of rotation of the shaft, which is equivalent to 5.5 milliseconds. Decreasing the time that the injector is open does not decrease the time it takes for the needle to transition from closed to open and back from open to closed.

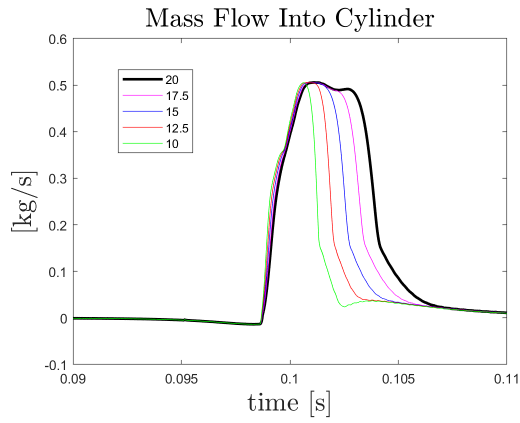


Figure 52: Mass Flow for Changing Injection Duration

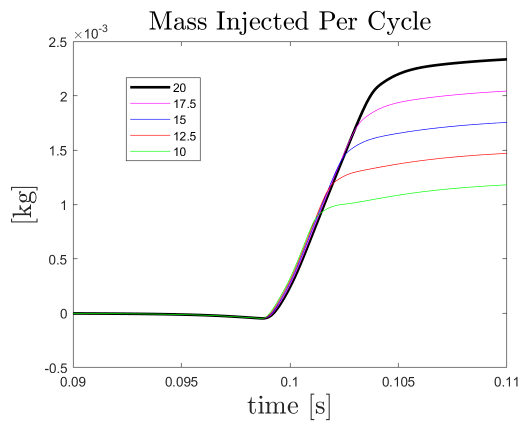


Figure 53: Mass Injected Per Cycle for Changing Injection Duration

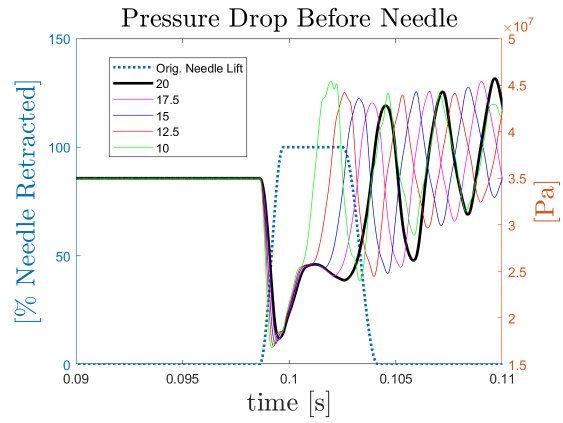


Figure 54: Pressure Drop During Injection for Changing Injection Duration

## 10.4 Failure Analysis

Two possible failure modes for this high pressure gas fuel injector. These include the cases where the injector needles become stuck in either the open or closed position. One or more needle stuck open can result in an over-rich mixture in the cylinder as well as a buildup of volatile fuel in the exhaust manifold. The consequences of a needle stuck in the closed position are less dangerous and are likely to be limited to a slight power reduction.

### 10.4.1 Closed Needle Comparison

Fuel flows through the injector between elements modeled as pipes and volumes. The final pipes, or channels, the gas moves through before injection into the cylinder are labeled as Pipe 3\_1 through 3\_6 in the image below.

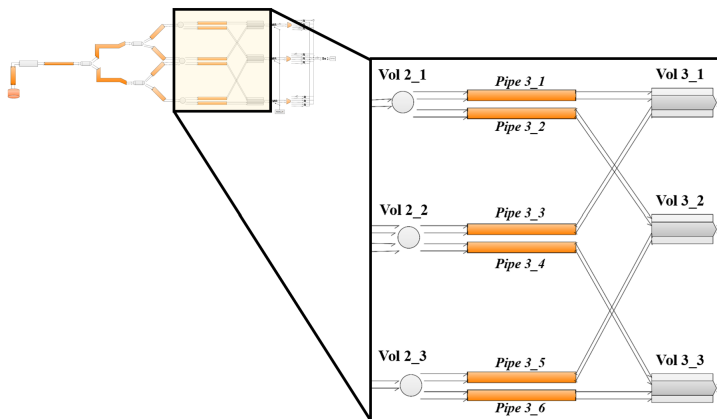


Figure 55: 20-Sim Model Components of Six Pipes Feeding Injector Needles

A simple observation of how gas flow splits through the six parallel pipes feeding the three injector needles shows that the flow is not identical across all the pipes. Pipes 1 & 6, 2 & 5, and 3 & 4 share the same gas velocity and mass flow in the fully operational condition. Despite this imbalance, the mass flow past each of the three needles is the same. If one needle were to stick closed, however, it is of interest to know if the compensated response differs if the failed component is the inner or an outer needle. The following plots show a comparison in the mass flow both out of the individual needles and into the cylinder for the cases where either an outer (Needle 1) or inner (Needle 2) needle is stuck in the closed position. The initial spike seen in Figure 57 is not seen in Figure 56 because some mass accumulates in the pre-cylinder volume before injection thus smoothing out the flow.

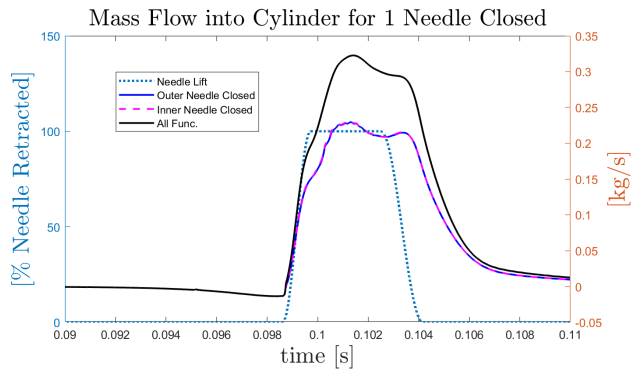


Figure 56: Comparison of Mass Flow into Cylinder for Inner vs. Outer Needle Stuck Closed

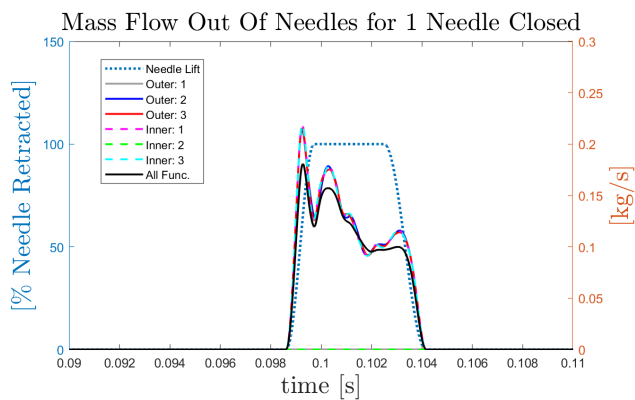


Figure 57: Comparison of Mass Flow Out of Individual Needles for Outer vs. Inner Needle Stuck Closed

These results indicate that differentiating between an outer or inner failed needle is not necessary for the forthcoming failure analyses because the compensated response for either of these cases is identical.

### 10.4.2 Mass Flow Considerations

If one or more needles of the three for each injector became stuck closed, there would logically be a power loss in that cylinder that could be compensated for by increasing the diesel pilot fuel flow if the failure was identified quickly and accurately. There may also be increased flow through the other two ports, however, so determining the right amount of pilot fuel to inject to compensate for this failure requires more detailed simulations. Several trials were run to investigate how one or two unresponsive needles contributed to an overall change in gas flow into the cylinder.

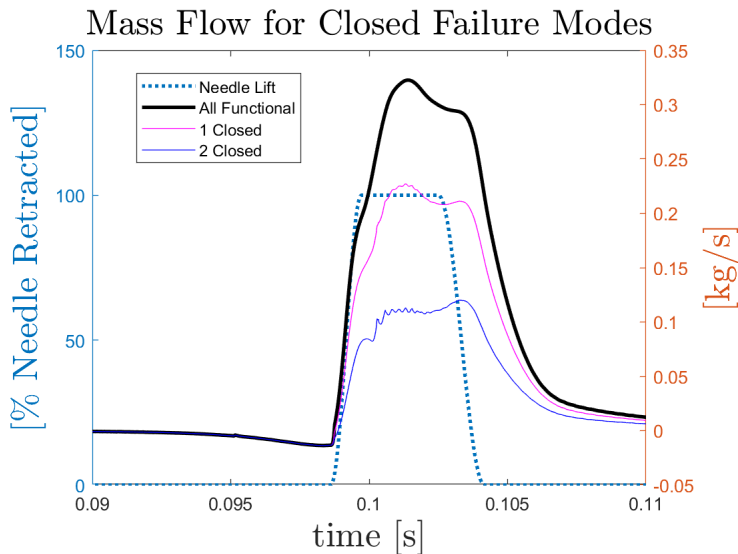


Figure 58: Mass Flow into Cylinder Comparison for Closed Needle Failure

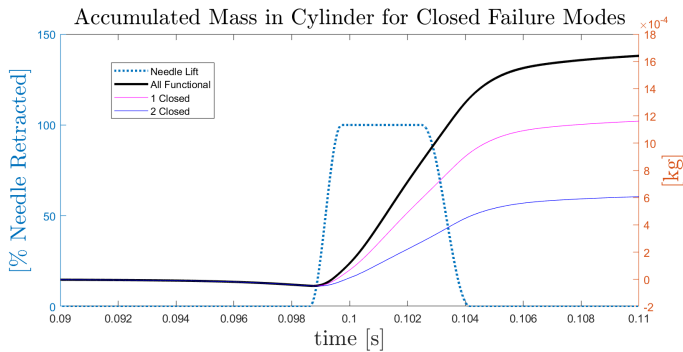


Figure 59: Mass Accumulated in Cylinder for Closed Needle Failure

These results indicate that when one or two needles fails to open during injection, there is no significant compensation for the reduced mass flow from the functional needle or needles. Mass flow through each needle remains constant despite the fact, which will be shown later, that upstream pressure increases slightly when a needle fails to open.

In the alternative case, if one or more needles becomes stuck in the open position, the potential for a dangerously rich mixture in the cylinder exists that may result in catastrophic equipment failure. Considering the fact that an advantage of direct-injection gaseous fuel is that it offers the potential of drastically reducing unburnt fuel emissions means that failing to detect an injector failure in the open position and secure the component would result in excessive harmful emissions and a potentially combustible mixture residing in the exhaust manifold.

When a needle fails in the open position, Figure 60 below indicates that the mass flow into the cylinder stabilizes just below half of the maximum mass flow during injection when just one needle fails and close to the maximum mass flow when two needles fail.

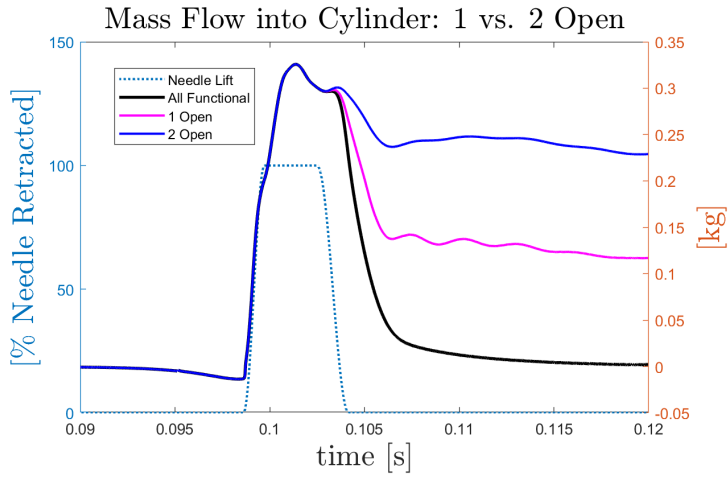


Figure 60: Mass Flow Comparison for Open Needle Failure

This increase in mass flow translates to an accumulated mass in the cylinder many times over the amount injected in one cycle. This indicates that a dangerous condition in the cylinder and the exhaust manifold could result very soon after failure, so early detection is vital.

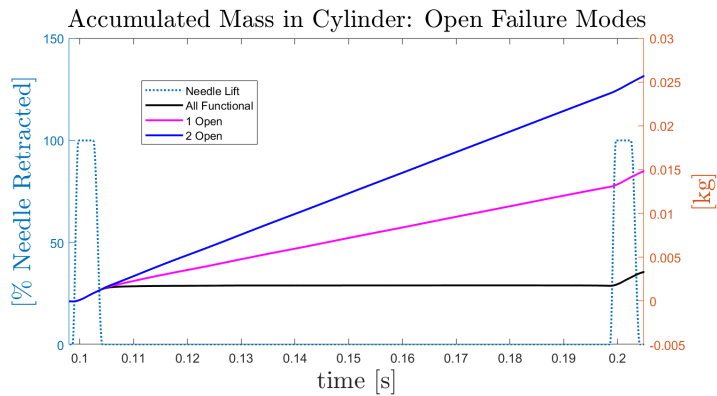


Figure 61: Mass Accumulated in Cylinder for Open Needle Failure

### 10.4.3 Pressure Drop and Quick Closing Valve

A safety cut-off switch is proposed that would stop the gas supply if a specified amount of downstream pressure is not maintained. If all injector needles are functioning properly, pressure inside the injector should drop briefly during injection but rapidly return to the upstream pressure after injection concludes. If a needle were to stick in the open position, the downstream pressure may not increase to the same level after injection and the safety closing valve would then activate to prevent excessive gas buildup in the cylinder.

The image below shows the operation of this proposed quick closing valve. The downstream pressure (a) extends the spring to expose the opening at (b). When sufficient downstream pressure exists, gas flows into the cylinder through the route shown by (c).

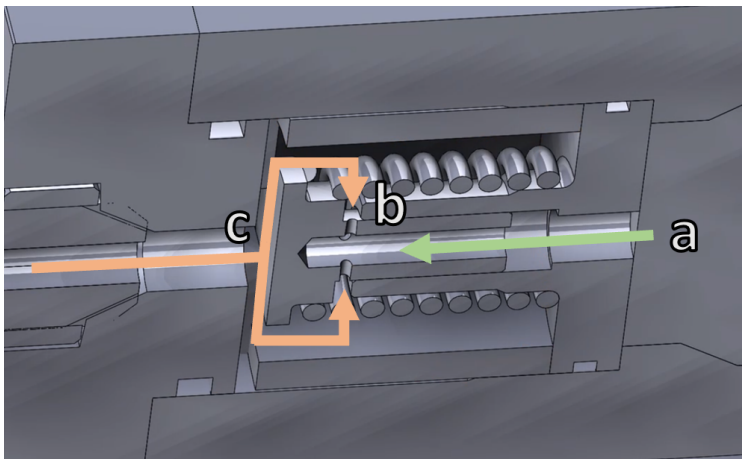


Figure 62: Proposed Quick Closing Valve Actuation

This concept was tested for viability by investigating how the pressure in the uppermost volumes of the injector changes for the conditions where one or two

needles becomes stuck open. These volumes were selected for initial examination because it is assumed that greater constraints on injector geometry exist in the lower portion of the injector, so installing the safety device there would be more challenging. The first two injections after the failure are shown in the following plots.

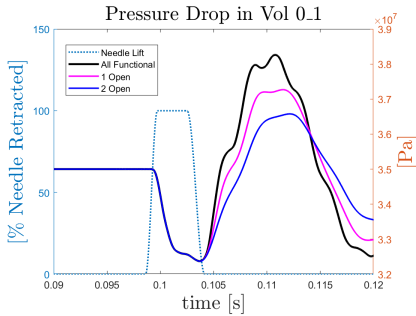


Figure 63: First Injection

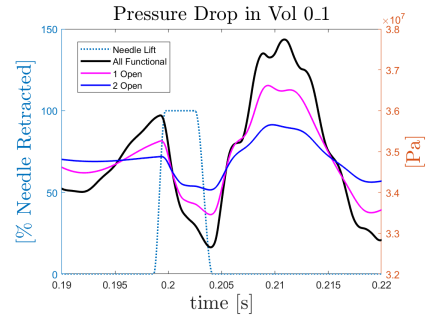


Figure 64: Second Injection

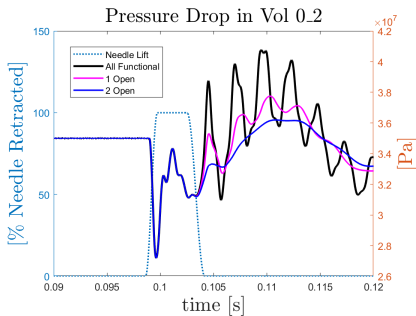


Figure 65: First Injection

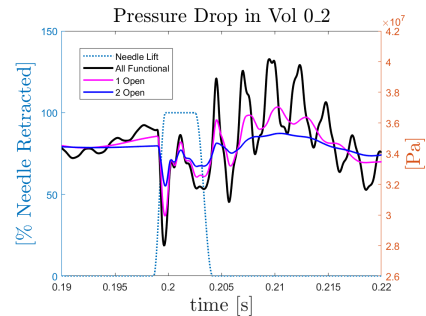


Figure 66: Second Injection

It is impossible to distinguish between the failed and functional conditions on the first injection, but on the second and subsequent injections, a smaller pressure drop is observed in both Volume 0\_1 and 0\_2 during injection. Additionally, the pressure fluctuations in each of these volumes have greater amplitudes in

the functional condition, which makes the simple spring-actuated safety switch difficult if not impossible to implement in either of these volumes.

If the proposed quick closing valve is used in this application, it would be more likely to shut off the gas supply in normal operation than during a failure when one or more needles remains open between injection cycles. It has already been shown that the mass flow out of each needle is constant whether the needle is functioning alongside either functional or non-functional needles. This result is consistent with the pressure drop data since a reduction in mass flow logically occurs with a decrease in pressure drop in the injector. Furthermore, the large pressure fluctuations both above and below the steady-state pressure level indicate that the quick closing valve's pressure set point would need to be so far outside the normal range that it would be rendered useless.

While detection of this failure in the first or second injection would be ideal, it is also of interest to understand how the pressures in these volumes stabilize during an open-needle failure. If the steady-state pressure during an open needle failure is consistently lower than the pressure in the functional condition, detection and shutoff could possibly occur with this proposed device. The pressure fluctuations stabilize to their new levels after three injection cycles with one or two needles failed in the open position, so the following plots show just the second and third injection after failure occurs.

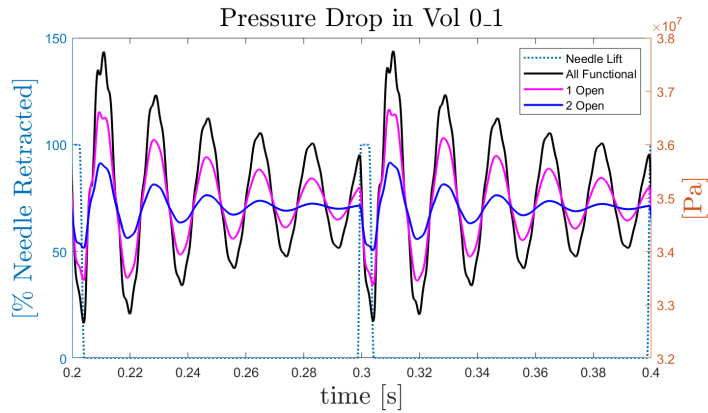


Figure 67: Pressure in Volume 0\_1 With Failure: Steady State

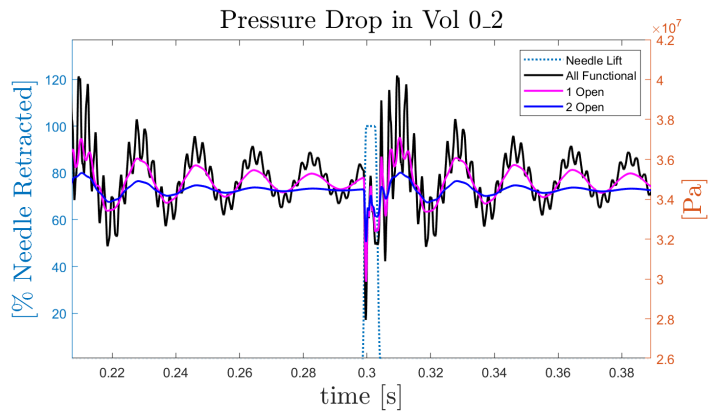


Figure 68: Pressure in Volume 0\_2 With Failure: Steady State

Based on the pressure fluctuations observed in both volumes in these simulations, it does not appear to be practical to install a pressure-actuated quick closing device in either of the locations focused on here. The actuation of such a device requires consistent downstream pressures at a lower level than occurs in normal operation. The simulations show that the pressure fluctuations occur-

ring in the fully functional condition may be both higher and lower than the sustained downstream pressure if one or two needles is stuck in the open position. If the safety valve was installed, it would rapidly open and close many times between injections as pressure dropped below the spring's required tension to remain open. Additionally, when a needle is stuck in the open position, the pressure drop during injection is shown in Figure 64 to actually be less than in the fully functioning condition. Thus, the overall principle of this safety device is ineffective for this application.

#### 10.4.4 Gas Velocity

In order to gain a deeper understanding of how flow inside the fuel injector changes when there is an injector needle failure, the gas velocity at the center of the six channels in the injector was analyzed.

The figure below shows the three pairs of matching velocity across the six main channels feeding the volumes just before the injector needles. It was previously stated that despite the three pairs of velocity values observed in the pipes during injection, the mass flow through each needle is equivalent. Analyzing the plot below reveals that the average of the highest and lowest velocities observed is the same as the median velocity. Thus, when the flows combine in Volumes 3\_1, 3\_2, and 3\_3, the resulting mass flow is the same.

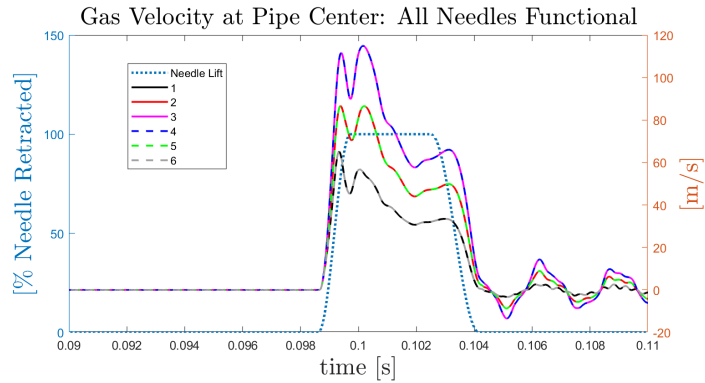


Figure 69: Gas Pipe Velocity: Fully Operational Condition

When Needle 1 is closed, the velocity in Pipe 1, which normally only feeds Needle 1, reverses as flow is redistributed to the other two needles. Additionally, the maximum velocity observed in Pipe 3 decreases for the same reason, although it does not reverse direction. These observations lead to the conclusion that gas flows through Pipe 3 into the pre-needle chamber then backwards through Pipe 1 to be redistributed to the other needles. The maximum velocity in Pipes 2 and 4 increases to compensate for the reduction in flow through Pipes 1 and 3.

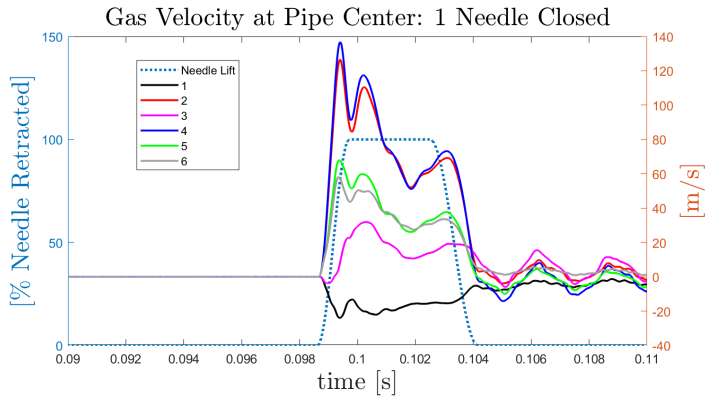


Figure 70: Gas Pipe Velocity: 1 Injector Needle Stuck Closed

When 2 needles are closed, similar effects are observed as flow reverses to supply the functional Needle 3. The maximum velocity observed when one needle fails closed is equivalent to the maximum velocity when two fail closed. This indicates that flow restrictions in the different internal components of the injector prevent flow from increasing through the still functioning injectors to compensate for the failure.

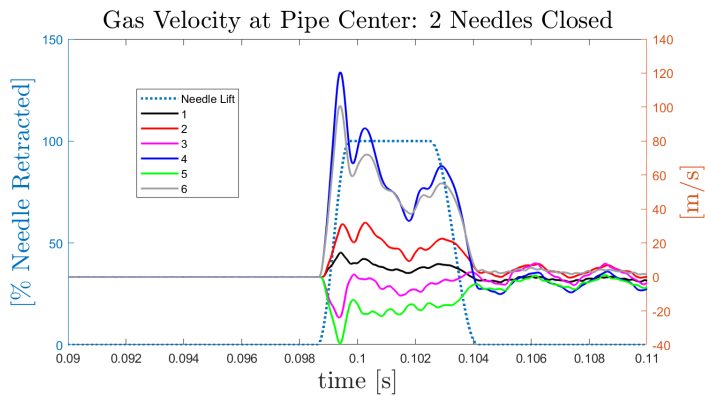


Figure 71: Gas Pipe Velocity: 2 Injector Needles Stuck Closed

When either one or two needles is stuck in the open position, there is always some velocity in the pipes.

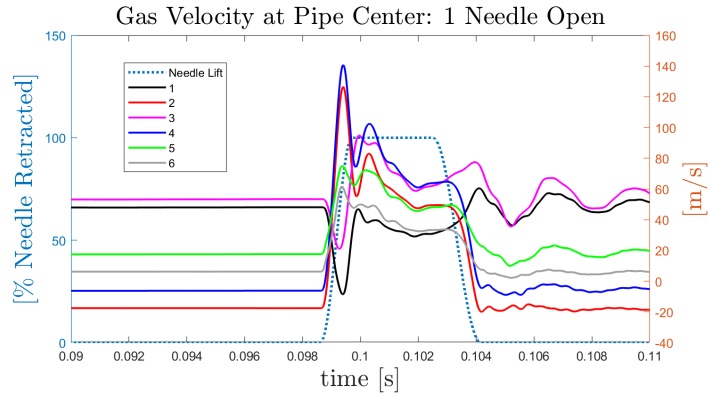


Figure 72: Gas Pipe Velocity: 1 Injector Needle Stuck Open

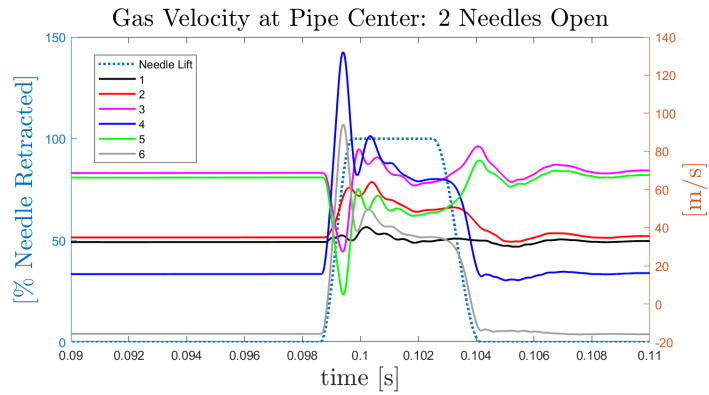


Figure 73: Gas Pipe Velocity: 2 Injector Needles Stuck Open

---

## 11 Summary

The high pressure fuel injector design reviews conducted for this thesis used 20-Sim models built using bond graph theory to simulate gas dynamics for this novel emissions-reducing technology. Starting with a simpler model facilitated early discovery of significant relationships between internal volumes and flow properties. When a more advanced injector drawing was made available, a new model was created and tested for more advanced performance properties. Furthermore, investigation into failure modes, detection methods, and consequences were quantified and a proposed safety device was evaluated.

### 11.1 Conclusions

#### 11.1.1 Simple Model

Analysis of injection cycle simulations using the initial simple model reveal that changing the pipe volume has a more significant effect on the parameters of focus than changing any other internal dimension. The primary parameters investigated for this design review were mass flow into the cylinder and pressure waves within the injector. Increasing the pipe volume in this model resulted in a very slight reduction in the pressure wave frequency in the system and had little effect on the mass flow into the cylinder. Decreasing the pipe volume by 40% resulted in doubling the pressure drop during injection and a reduction in mass flow by approximately 50%. The fact that significant changes were seen for reducing the pipe size but not increasing it leads to the conclusion that the current

size is the smallest acceptable without additional component tuning to ensure adequate performance of the injector.

Analysis of pressure waves in the several components of this simplified model revealed that the fluctuations observed are not a result of a resonant frequency of the pipe but rather are common throughout the system. When the pressure each control volume within the pipes was plotted and compared, it became apparent that the pressure within the pipes is close to consistent and any pressure fluctuations occur simultaneously throughout the pipe. These fluctuations are a result of the high pressure the system exists under and the need for rapid refilling of the injector with gas from upstream between injection cycles. When the injector is exposed to the lower pressures downstream during injection, the pressure differential that exceeds 2:1 both drives efficient injection and results in pressure waves between cycles.

The original hypothesis that the pipe dimensions would drive the frequency of pressure oscillations in the system was false. Simulations showed that the pressure oscillations exist consistently throughout the system and the gas pressure within the individual pipes oscillates together rather than as a wave. The largest volumes in the injector, regardless of shape, were shown to influence both pressure fluctuations and mass flow into the cylinder.

### **11.1.2 Advanced Model**

The advanced model was assumed to have similar properties for gas flow in the spaces modeled as pipes as the simplified model, so changing the spaces where gas accumulated (the capacitor elements of the model) was the focus of the design review of this new model. Increasing and decreasing each of these volumes

by factors of two and four revealed that the sac volume is the only one that produces significant changes in the mass flow of fuel into the cylinder. The other intermediate volumes between the supply and the cylinder are available to be tuned as needed to accommodate space concerns or machine limitations during production.

Changing the upstream pressure was proven to have a proportional response on the mass flow out of the injector. Slight decreases from the assumed 350 bar standard are acceptable, but decreases below 300 bar may have a significant effect on the power produced by the engine. Changing the duration of injection was found to have a similar proportional response.

Several failure modes were investigated and it was shown that failure of an injector needle to close after injection results in a dangerous condition within just one cycle. The proposed safety device relies on detection of reduced downstream pressure to function. The pressure drop during injection for a needle open failure is less significant than when the injector is fully functional. This means that the proposed device which requires a certain level of downstream pressure to admit gas into the cylinder would activate to restrict flow while the injector is fully functional, not when there is a failure.

### **11.2 Discussion and Further Work**

This thesis evaluated the effect of changing the internal dimensions of two fuel injector models on the mass flow into the cylinder and pressure fluctuations within the injector. Additionally, the assumptions that simplified the model including adiabatic and isentropic conditions were confirmed to be acceptable. The more advanced model that was developed and tested for this thesis may serve as a

starting point for future simulations and design verification as the injector transitions from concept to prototype. The primary concern moving forward is the design of a functional safety device that can detect a failure of an injector needle to close between cycles and secure gas flow quickly. The current safety valve proposed was not found to be adequate for this purpose. One alternative option is to install a flow meter slightly up stream of the injector. Flow between injections should be minimal, and if the sensor is placed close to the first volume of the injector it may detect fluctuations and reversing direction between cycles. If constant flow was observed by this sensor, that would be one way to indicate that a needle is stuck open. A significant weakness of this approach is the fact that it would rely on electronics rather than the mechanical operation of the proposed and infeasible device.

## Bibliography

- Beck, L. (2019), 'Marine engineering specialization project: High pressure dual fuel engine - evaluation of performance and emission potential by modeling and simulation'.
- Fevre, C. N. L. (2018), 'A review of demand prospects for lng as a marine transport fuel', <https://www.oxfordenergy.org/wpcms/wp-content/uploads/2018/07/A-review-of-demand-prospects-for-LNG-as-a-marine-fuel-NG-133.pdf?v=c2f3f489a005>. Accessed: 2019-12-08.
- GHGP (2018), 'Global warming potential values', [https://www.ghgprotocol.org/sites/default/files/ghgp/Global-Warming-Potential-Values%2028Feb%2016%202016%29\\_1.pdf](https://www.ghgprotocol.org/sites/default/files/ghgp/Global-Warming-Potential-Values%2028Feb%2016%202016%29_1.pdf). Accessed: 2019-11-01.
- IMO (2012a), 'Nitrogen oxides (nox) - regulation 13', [http://www.imo.org/en/OurWork/Environment/PollutionPrevention/AirPollution/Pages/Nitrogen-oxides-\(NOx\)-%E2%80%93Regulation-13.aspx](http://www.imo.org/en/OurWork/Environment/PollutionPrevention/AirPollution/Pages/Nitrogen-oxides-(NOx)-%E2%80%93Regulation-13.aspx).
- IMO (2012b), 'Sulphur oxides (sox) and particulate matter (pm) regulation 14', [http://www.imo.org/en/OurWork/Environment/PollutionPrevention/AirPollution/Pages/Sulphur-oxides-\(SOx\)--Regulation-14.aspx](http://www.imo.org/en/OurWork/Environment/PollutionPrevention/AirPollution/Pages/Sulphur-oxides-(SOx)--Regulation-14.aspx). Accessed: 2019-11-01.
- IMO (2019), 'Status of imo treaties', <http://www.imo.org/en/About/Conventions/StatusOfConventions/Documents/Status%20-%202019.pdf>. Accessed: 2019-09-20.
- IMO (2020), 'Energy efficiency measures', <http://www.imo.org/en/OurWork/Environment/PollutionPrevention/AirPollution/Pages/Technical-and-Operational-Measures.aspx>. Accessed: 2019-10-10.
- Jingzhou Yu, Ville Vuorinen, O. K. T. S. M. L. (2013), 'Characteristics of high pressure jets for direct injection gas engine', *SAE International Journal of Fuels and Lubrication* **6**(1).

- Karnopp, D. C., Margolis, D. L. & Rosenberg, R. C. (2012), *System Dynamics. Modeling, Simulation, and Control of Mechatronic Systems*, Wiley.
- Krivopolianskii, V. (2019), *Experimental investigation of injection and combustion processes in marine gas engines using constant volume rig*, Ph.D. Thesis, NTNU Department of Marine Technology, Trondheim, Norway.
- Marintek (2019), 'Design workshop on hpdf-gas injectors'.
- Ohashi, I. (2015), 'Dual-fuel marine engine (highly reliable environmentally friendly engine)', [https://www.yanmar.com/global/technology/technical\\_review/2015/0727\\_2.html](https://www.yanmar.com/global/technology/technical_review/2015/0727_2.html). Accessed: 2019-11-01.
- Senghaas, C. (2019), 'New injector family for high-pressure gas and low-caloric liquid fuels', *CIMAC Congress* .
- Strand, Kurt, E. H. (1991), 'Bond graph interpretation of one-dimensional fluid flow', *The Franklin Institute* **328**(5/6).
- Vilmar Aeligsoy, Per Magne Einang, D. S. E. H. & Valberg., I. (2011), 'Lng-fuelled engines and fuel systems for medium-speed engines in maritime applications', *SAE Technical Papers* .

# Appendices



---

## **A Model Input Parameters**

The parameters used in both versions of the fuel injector model are shown on the next page. These global parameters exclude the exact component sizes which can be found in the body of the report.

**Input Parameters for Simplified Model**

<b>Variable</b>		<b>Value</b>	
$\kappa$	<i>Heat Capacity Ratio</i>	1.41	-
$R_{gas}$	<i>Gas Constant</i>	518.28	J/ kg K
$T_{cyl}$	<i>Cylinder Temperature</i>	1000	K
$P0$	<i>Initial Injector Pressure</i>	350	bar
$T0$	<i>Initial Injector Temperature</i>	158	K
$fric$	<i>Friction</i>	0.02	-
$t_{factIM}$	<i>Isentropic Correction Coefficient</i>	0.061	-
$x_{fIM}$	<i>Adiabatic Correction Coefficient</i>	-0.062	-
$Cd$	<i>Discharge Coefficient</i>	0.8	-
$Cd$	<i>Discharge Coefficient</i>	0.8	-

**Input Parameters for Advanced Model**

<b>Variable</b>		<b>Value</b>	
$\kappa$	<i>Heat Capacity Ratio</i>	1.8	-
$R_{gas}$	<i>Gas Constant</i>	518.28	J/ kg K
$T_{cyl}$	<i>Cylinder Temperature</i>	1000	K
$P0$	<i>Initial Injector Pressure</i>	350	bar
$T0$	<i>Initial Injector Temperature</i>	300	K
$fric$	<i>Friction</i>	0.02	-
$t_{factIM}$	<i>Isentropic Correction Coefficient</i>	0.5	-
$x_{fIM}$	<i>Adiabatic Correction Coefficient</i>	-0.5	-
$Cd$	<i>Discharge Coefficient</i>	0.8	-
$Cd$	<i>Discharge Coefficient</i>	0.8	-

---

## B 20-Sim Pipe Code

The main portion of the code that calculated flow in the pipes of the 20-Sim models used in this thesis is copied below. The code is based on the formulas in the reference [Strand \(1991\)](#). Much of the code was developed by my supervisor, Professor Eilif Pedersen.

```
// Code block
code
    //integral of vector YP with the initial conditions as established above
Y = int(YP, YP0);

// Assemble states from state vector
for i=1 to N do
m[i+1] = Y[i*3-2]; //mass
mo[i+1] = Y[i*3-1]; //mass*velocity
E[i+1] = Y[i*3]; //mass*energy
end;

// State in control volume i:
lammax=0.0;
for i=1 to N do
u[i+1] = mo[i+1]/m[i+1]; //velocity
z[i+1] = u [i+1];
ro[i+1] = m[i+1]/vol; //density
t[i+1] = E[i+1]/(m[i+1]*cv); //temperature
p[i+1] = m[i+1]*rgas*t[i+1]/vol; //pressure
ht[i+1] = cp*t[i+1]; //enthalpy
c = sqrt(abs(kap*rgas*t[i+1])); //speed of sound
am[i+1] = abs(u[i+1])/c; //mach number
l1 =abs(u[i+1]+c);
```

```
l2 =abs(u[i+1]-c);
lam =max([l1,l2]); //spectral radius
lammax =max([lam,lammax]);
end;

// Boundary conditions
t[1] = Tin.e;
p[1] = Pin.e;
ro[1] = Pin.e/(rgas*Tin.e);

t[N+2] = Tout.e;
p[N+2] = Pout.e;
ro[N+2] = Pout.e/(rgas*Tout.e);

// Calculate internal flux value of variables
for i = 2 to N do
ui1 = (u[i+1]+u[i])*0.5;
dir=sign(ui1);

aam = (am[i]+am[i+1])*0.5+dir*(am[i]-am[i+1])*0.5;
if aam > 1.0 then
aa1=1.0; aa2=1.0; aa3=1.0; aa4=1.0;
else
aa1=aam^an1; aa2=aam^an2; aa3=aam^an3; aa4=aam^an4;
end;

ui[i] = ui1 + aa1*dir*(u[i]-u[i+1])*0.5;
pin[i] = (p[i+1]+p[i])*0.5 + aa2*dir*(p[i]-p[i+1])*0.5;
ti[i] = (t[i+1]+t[i])*0.5 + aa4*dir*(t[i]-t[i+1])*0.5;
hti[i] = (ht[i+1]+ht[i])*0.5 + aa4*dir*(ht[i]-ht[i+1])*0.5;
roi[i] = (ro[i+1]+ro[i])*0.5 + aa3*dir*(ro[i]-ro[i+1])*0.5;

dmi[i] = roi[i]*ui[i]*area;
dei[i] = dmi[i]*(hti[i]+0.5*ui[i]*ui[i]);
dfi[i] = pin[i]*area + dmi[i]*ui[i];
```

---

```

end;

// =====
// Left pipe end
// =====
p1 = p[2];
u1 = u[2];
t1 = t[2];
ro1 = ro[2];
c1 = sqrt(abs(kap*p1/ro1));
S1 = p1/(abs(ro1)^kap);
e1 = p1/(kap-1.0) + 0.5*ro1*u1*u1;
pBM= p[1];
tBM= t[1];

rL1 = u1 + c1;
rL2 = u1;
rL3 = u1-c1;

tilfelle=if rL2 <= 0 then //tilfelle = case
if rL1 > 0 then
1
else
2
end
else
if rL3 < 0 then
3
else
4
end
end;
if WallM == 1 then
tilfelle=0;

```

---

```
end;

switch tilfelle
case 0 do
// Pipe end Left closed
cB = c1 - (kap-1)/2*u1;
rB = (cB*cB/(kap*S1))^(1.0/(kap-1.0));
pB = cB*cB*rB/kap;

dmif = 0.0;
deif = 0.0;
dfif = pB*area;
case 1 do
// Subsonic flow out
pB = pBM;
rB = ro1*(pB/p1)^(1.0/kap);
    cB = sqrt(abs(kap*pB/rB));
    uB = u1-2.0/(kap-1.0)*(c1-cB);
    eB = pB/(kap-1.0) + 0.5*rB*(uB^2);
    dmif = rB*uB*area;
    deif = (eB+pB)*uB*area;
    dfif = (rB*uB*uB+pB)*area;
case 2 do
// Supersonic flow out
    dmif = ro1*u1*area;
    deif = (e1+p1)*u1*area;
    dfif = (ro1*u1*u1+p1)*area;

case 3 do

// === Subsonic flow in
    cp = kap*rgas/(kap-1.0);
    Tny = tBM-tfactlM*0.5*u1*u1/cp;
pny = pBM*(Tny/tBM)^(kap/(kap-1.0));
```

---

```

        if xflM < 0.0 then
// === Isentropic assumption
            pny = pBM*(Tny/tBM)^(kap/(kap-1.0));
            else
// === Adiabatic assumption
            red = 0.5*xflM*u1*u1/(rgas*Tny);
            pny = pBM/(1.0+red);
end;
```

```

rny = pny/(rgas*Tny);
pB = pny;
rB = rny;
SB = pB/(rB^kap);
cB = sqrt(kap*pB/rB);
prsI = p1;
uI = u1;
rI = (prsI/SB)^(1.0/kap);
cI = sqrt(kap*prsI/rI);
uB = u1-2.0/(kap-1.0)*(cI-cB);
eB = pB/(kap-1.0) + 0.5*rB*(uB^2);
```

```

dmif = rB*uB*area;
deif = (eB+pB)*uB*area;
dfif = (rB*uB*uB+pB)*area;
```

```
case 4 do
```

```

// === Supersonic flow in
    pB = pBM;
    rB = pB/(rgas*tBM);
    uB = sqrt(kap*rgas*tBM);
    eB = pB/(kap-1.0) + 0.5*rB*(uB^2);
```

```

    dmif = rB*uB*area;
    deif = (eB+pB)*uB*area;
    dfif = (rB*uB*uB+pB)*area;
```

```
end;

// Assign flux value for left pipe end

pin[1] =pB;
  dmi[1] = dmif;
  dei[1] = deif;
  dfi[1] = dfif;
```

The same code repeats for the right pipe end to make the model capable to calculating flow in either direction. The last step of the pipe model is to assign fluxes to each end of the pipe where it connects to the neighboring elements.

```
//-----
// Calculate net flux rates, i.e mass, energy and momentum,
into control volume no i:
//-----

for i = 1 to N do
ii=i+1;
YP[3*i-2] = dmi[i] - dmi[i+1];
YP[3*i-1] = dfi[i] - dfi[i+1] - 0.5*fric*m[ii]*u[ii]*abs(u[ii])/diam;
YP[3*i] = dei[i] - dei[i+1];
end;
// Set pipe end fluxes, here only mass and energy

Pin.f = dmi[1];
Tin.f = dei[1];

Pout.f = dmi[N+1];
Tout.f = dei[N+1];

mydt=stepsize;
myCFL=dx/lammax;
```

